2006:20

LICENTIATE THESIS

L

Towards a Measurement of Paper Pulp Quality: Ultrasonic Spectroscopy of Fibre Suspensions

Yvonne Aitomäki

Luleå University of Technology
Department of Computer Science and Electrical Engineering
EISLAB

2006:20 | ISSN: 1402-1757 | ISRN: LTU-LIC -- 06/20 -- SE

Towards a Measurement of Paper Pulp Quality: Ultrasonic Spectroscopy of Fibre Suspensions

Yvonne Aitomäki

EISLAB
Dept. of Computer Science and Electrical Engineering
Luleå University of Technology
Luleå, Sweden

Supervisor:

Torbjörn Löfqvist, Jerker Delsing

European Union
Structural Funds

Dedicated to the memory of Bernard Schlecht who taught me to climb

and inspired me to study

Abstract

For the paper and pulp industry in Sweden and Finland to remain competitive against countries with lower overheads, they have to constantly strive to improve the quality and the efficiency of the manufacturing processes. One of the ways of doing this is to introduce sensors that will provide valuable online feedback on the characteristics of the pulp so that adjustments can be made to optimise the manufacturing process. The measurement method proposed in this thesis is based on ultrasound, since it is rapid, inexpensive, non-destructive and non-intrusive. Thus could be done online. Since ultrasound propagation and attenuation depends on the material properties through which is propagates, it has the potential to provide measurements of material properties such as pulp fibre density and elasticity.

The aim of this thesis is to investigate the possibility of using ultrasound to measure pulp fibre material properties. The idea is to solve the inverse problem of estimating these properties from attenuation measurements and to establish the degree of accuracy to which this can be done. Firstly a model is developed and is tested with synthetic fibres to establish is validity. It is then used to solve the inverse problem of estimating material properties from attenuation measurements, again with synthetic fibres, to test the accuracy to which these properties can be estimated. Resonance peaks in the frequency response of the attenuation were found. On closer investigation it was established that the location of these peaks in the frequency domain is sensitive to the diameter of the fibres and their material properties. If the diameter is known, these peaks improve the accuracy of the estimation process. The results of the estimation process for synthetic fibre suspensions show values for the shear modulus are within known ranges but the estimation of Poisson's ratio and Young's modulus is poor. Improving the model or the estimation procedure may lead to better results.

For the method as it is to have application in the paper and pulp industry there are certain conditions that need to be fulfilled. These are that we find peaks in the frequency response of the attenuation in pulp, know the diameter distribution of the fibres and the hollow nature of the fibres does not significantly alter the results. We can then, potentially, be able to establish the shear modulus of the pulp fibres. If the shear modulus is a factor in paper quality, we may be close to an online measurement of paper pulp quality using ultrasonic spectroscopy. Improving the model may allow us to estimate further properties and take into account the fibres being hollow.

The thesis consists of two parts. The first part includes an overview of the pulp and paper industry and current testing methods, background theory on which the model is based and an overview of the model that is used in predicting ultrasound attenuation.

There then follows a summary of the work done, some addition points are raised in the discussion before drawing conclusions. Finally we discuss what needs to be done to take this further. The second part contains a collection of four papers describing the research.

Contents

Acknowledgements

I would like to thank my supervisor Torbjörn Löfqvist, for his comments and support. I would also like to thank Jerker Delsing for reminding me of the big picture. Thanks also to my friends and colleagues at CSEE for their support and patient nodding as I rant on about waves, boundary conditions and about the fact that I've done it wrong - oh no its all okay again etc, etc. I would especially like to thank Kristina Berglund, who has shown amazing flare at correcting my English and has patiently gone through version after version of this thesis and most importantly come up with the elastic band analogy. Appreciation also goes the Forskningskola för Kvinnor, for giving me the confidence to forge ahead and for the laughing therapy.

Finally my special thanks goes to my husband, Erik, without whose support I could not have done this. And my Mum and Dad for the proof-reading and comments.

Part I

Chapter 1

Introduction

In 2005, Sweden produced 11.7 million metric tons of paper and pulp. In 2002, Finland and Sweden were the third and fourth largest producers of paper and pulp and together they make up for 12% of the world's paper and pulp production. With an annual turnover of EUR 74 billion, the pulp and paper industry is a vital part of the European paper and forest economic cluster[1].

For the paper and pulp industry in Sweden and Finland to remain competitive against countries with lower overheads, they have to constantly strive to improve the quality and the efficiency of the manufacturing process. In 2000, the paper and pulp industry was responsible for 2% of the primary energy consumption of the EU's twelve member states. The high cost of energy in Europe make improvements in energy efficiency a considerable cost saving. The balance is then to reduce the energy consumption whilst maintaining quality. Hence the need for improving process control.

A large number of instruments exist for measuring different aspects of pulp, such as the brightness, chemical analysis, consistency and fibre properties [2]. With the increase in computer processing power, rapid image analysis has allowed optical measurement techniques to become standard practice in the paper and pulp manufacturing process in Scandinavia. Examples of devices that use optical-based image analysis are the STFI Fibremaster, (Lorentsen-Wettre, Sweden) and the Kajaani FS300 (Metso Automation, Finland). Although they provide valuable information on a number of fibre properties, since the method is optical, material properties such as elasticity cannot be measured. Or, in layman's terms 'No matter how much you stare at an elastic band, you still don't know how stretchy it is´.

A recent development in the online measurement of paper quality control is the use of a laser ultrasonic sensor (Berkeley Lab, Berkeley, California). This measures the bending stiffness and out-of-plane shear rigidity. Trials using this device started in 2003.

This device is an example where material properties can be estimated using ultrasound since they affect the attenuation and wave speed of the ultrasonic wave as it progresses through the material. Hence the use of ultrasound measurement methods can provide rapid, inexpensive, non-destructive and non-intrusive measurements. Historically, there

have been a number of attempts to introduce ultrasonics into the paper and pulp industry but up until 1998 these were without much success. A summary of these is given by [3]. One of the reasons given was the emphasis the industry had on quantity rather than quality. The economic climate, at least in Europe, has changed and it would seem that the emphasis is now on quality and efficiency. The indications for this are from the widespread use of optical devices for monitoring pulp in Scandinavia. However, the correlation between optical fibre characteristics and paper quality has had variable success [4]. This is perhaps because fibre material property measurements are missing. In this case ultrasound based measurements could have the potential to provide the key to increased process efficient by supplying this missing data.

The aim of this thesis is to investigate the possibilities of being able to use ultrasound to estimate the material properties of pulp fibres in suspension. The material properties we intend to measure are the shear modulus, Young's modulus and density.

Given this feedback, one can envisage the paper manufacturing plant of the future having ultrasonic devices for measuring density and elasticity at each stage in the pulp making process. Each stage could then be adjusted to the type or condition of the wood fibre being fed into the process. The plant would have an online paper quality measurement device, such as the laser ultrasonic sensor, to correlate the information on the individual fibre properties, at each stage in the process, with the output quality of the paper.

The thesis is composed of two parts: firstly a general background and secondly papers that have been either published or submitted for publication. The general background is divided into an overview of the paper manufacturing process and current testing methods in paper pulp. Some aspects of the physics of ultrasound propagation are discussed before presenting the historical background on the modelling of ultrasound propagation in suspensions. We then present an overview of the simple cylinder scattering (SCS) model and a summary of the papers is given in Chapter 4. We discuss some additional issues not tackled in the papers before drawing conclusions. Finally we discuss what needs to be done to take this further. The second part contains a collection of four papers describing the research.

Chapter 2

Paper and Pulp Industry

2.1 Paper and Pulp Manufacturing Process

There are three basic types of pulp manufacturing: chemical, mechanical and pulp from recycled paper. In the chemical pulp manufacturing process, the wood is cooked in a solution of chemicals. The lignin of the wood is made soluble and the fibres separate as whole fibres. In mechanical pulp manufacturing, the wood fibres may also be exposed to heat and pressure, such as in thermomechanical pulps, [5], before being separated by grinding or milling. An overview of these different processes is provided in [6].

2.2 Current Methods of Pulp Quality Measurement

Due to the large number of different factors that contribute to make paper to the desired specifications, the main method of testing paper pulp quality is to making the pulp into paper and testing the resulting paper [7]. This can be done in laboratory setting to assess differences due to wood types or different treatment processes and more recently, the effects of recycling [8].

There is a whole plethora of devices available for monitoring the pulp at different stages of the process. Devices are available for measuring fibre consistency, chemical composition, brightness, yield, and visual features of the fibre that can be measured using optical devices. Some of which, like the optical devices, are available online. Definitions of these qualities are given in [2]. If we concentrate on the measurement techniques or devices available for measure Young's modulus, density and shear modulus, the list of available devices and techniques are considerably shorter.

The stiffness of individual fibre can be measured and through this Young's modulus established. The first of the two main method used is done by setting the fibre in a v-shaped notch on the tip of a thin capillary tube submersed in water. Water is then allowed flow through the capillary. This water flow is increased until the middle part of the fibre reaches a preset mark [2]. The second method is to measure the extent to which

a fibre has followed the contour of a wire set between the fibre and a glass plate, when a hydraulic pressure is applied. This process has been automated and is available [2].

The SFTI fibremaster, gives an indication of the stiffness through a measurement quantity referred to as bendability. This is defined as the difference in form factor when measured with high and normal flows in the STFI measuring cell. The form factor is the ratio of the greatest extension of the fibre to the real length of the fibre in the same projected plane [9]. The greatest extension is the degree of extension in the projected plane in which the fibre has its greatest bending. The use of flow and optical measurement, results in the ability of the system to provide a measurement related to the elasticity of the fibre. One of the problems with this method is that the fibre is projected onto two dimensions so that deflection in the third dimension is not considered and hence a source of inaccuracy in the measurement.

Methods or devices measuring the fibre material density in industrial setting have not been found. However, assessment of wood fibre density have been investigated by submerged float techniques by [10]. These results showed that the density is changed by the degree of delignification upto 20%. Hence chemical processes do affect the density of the fibre material. The density of the fibre structure depends to a large extent on the wall thickness. If this collapses the fibre will be denser. Measurement of fibre wall thickness are made by optical devices, such as the Fibermaster, and coarseness values are calculated where coarseness is the mass per unit length.

Measurements of shear modulus have not been found for pulp fibres.

Chapter 3

Ultrasound in Suspensions

3.1 Overview

Ultrasound is simply sound with higher frequencies than that the human ear can detect (>20kHz), hence theories on audible sound also apply to ultrasound. As sound propagates through a medium its amplitude decreases as the energy in the wave is absorbed. If the sound is a pulse then it will contain different frequencies and the shorter the pulse, the more frequencies it will contain. Sound waves with different frequencies are absorbed, or attenuated, by different amounts depending on the medium. In fluids, the classical explanation for attenuation is that it is due to the viscosity of the fluid as well as to thermal conduction. For non-metallic fluids, the attenuation due to thermal conduction is negligible compared to that due to viscosity [11]. Unfortunately for most common liquids this does not account for all the attenuation mechanisms. In water, this excess attenuation is attributed to structural relaxation. An additional viscosity term, bulk viscosity, is therefore introduced to take this into account. The resulting relationship for the attenuation in terms of the material properties is

$$\alpha \approx \omega^2 \left(\frac{\eta'}{B}\right) \frac{\sqrt{\rho_1}}{2}, \tag{3.1}$$

$$\eta' = \frac{4}{3}\eta + \eta_B, \tag{3.2}$$

where B is the adiabatic bulk modulus, ω is the angular frequency, ρ_1 the density of water and η is the viscosity and η_B is the bulk viscosity. For water, η_B is approximately three times that of the η. From equation (3.1) we see that as frequency increases the attenuation increases proportional to frequency squared.

In solids, the attenuation per wavelength can be approximated to the phase difference the stress and the strain, also referred to as the loss tangent, $\tan\delta$ [12] [13]. Stress and strain are related by the elastic modulus, M. To model the phase difference between

then, we let M become a complex number such that

$$M = M' + iM'' \tag{3.3}$$

and

$$\tan\delta = \frac{M'}{M''} \tag{3.4}$$

In terms of attenuation of the solid, α_f, this becomes

$$\alpha_f = \frac{\pi f}{c_2}\tan\delta \tag{3.5}$$

The mechanism by which the wave propagates through a medium depends on its material properties. In a fluid that is not close to any boundaries, the wave velocity, c_1 depends on the adiabatic bulk modulus and the density of the fluid (see equation (3.6)). It also has a term depending on the frequency of the wave squared and a function of the ratio of the viscosity to the adiabatic bulk modulus squared. As the frequency increases so does the velocity, but the ratio of the viscosity to the bulk modulus is small ($\approx 2\cdot 10^{012}$), the effect is less noticeable than the effect the frequency has on attenuation in a fluid. The equation for this relationship is:

$$c_1 \approx \sqrt{1+\frac{3}{8}\omega^2\left(\frac{\eta'}{B}\right)^2} \tag{3.6}$$

The approximation in this last expression and that for attenuation in a fluid, equation (3.1), is because this assumes that the term $\eta'/B \ll 1$.

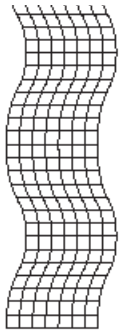

(a) Shear wave

Figure 3.1: Diagram of a shear wave propagating a solid.

If we consider wave motion in an unbound solid two types of waves can exist: a compressional wave and a shear wave. The shear wave is a transverse wave, where

the particle motion is perpendicular to the direction of propagation, as shown in the diagram in Figure 3.1. The wave depends only on the shear modulus of the material. The compressional wave is a longitudinal wave where the particle motion is in the same direction as the direction of propagation of the wave. If a sinusoidal force acts on a surface such that it is evenly compressed, as shown in Figure 3.2, then the velocity of the wave generated depends on Young's modulus. However, if the surface is not evenly compressed, such as is generally the case in an unbound solid, then both compression and shear waves will occur. Further details can be found in [14]. In the analysis in the model, we assume that the shear wave is perpendicular to the compression wave [15]. We can visualise this by imagining a plate in a soft solid, such as a gel. If a transverse wave is generated in the plate, and as a point in the plate moves up and down it compresses and expands the gel above it. This generates a compression wave perpendicular to the transverse wave. The velocity of this compression wave depends on the shear modulus, and on the bulk elasticity of the material. The bulk elasticity is used in place of Young's modulus because we cannot assume that the surfaces perpendicular to the applied stress are now free to move [14].

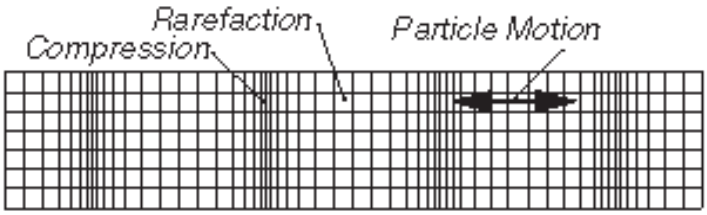

(b) Compression wave

Figure 3.2: Diagram of a pure compression wave propagating through a solid.

The equations for these relationships are:

$$c_{2_s} = \sqrt{(\mu/\rho_2)} \tag{3.7}$$

$$c_2 = \sqrt{((K + \frac{4}{3}\mu)/\rho_2)} \tag{3.8}$$

where c_{2_s} is the shear wave velocity, μ is the shear modulus, and ρ_2 is the density of the solid. c_2 is the compressional wave velocity, and K is the bulk modulus. When a solid medium is unbound we assume that the waves in the solid will be the combined compression and shear waves. Dispersion is taken into account, as the elastic modulii are complex as described earlier in the definition of the loss tangent.

The diagrams in Figure 3.1 and Figure 3.2 show the effect on an element of a solid. If we now imagine an infinitely long cylinder that is excited evenly along its z axis, from a particular point in (x,y), the displacement will be a shown in Figure 3.3. From this kind of excitation we can expect that both compression and shear waves will propagate in the cylinder. Complications do arise however, because of the boundary. This will be discussed at a later point.

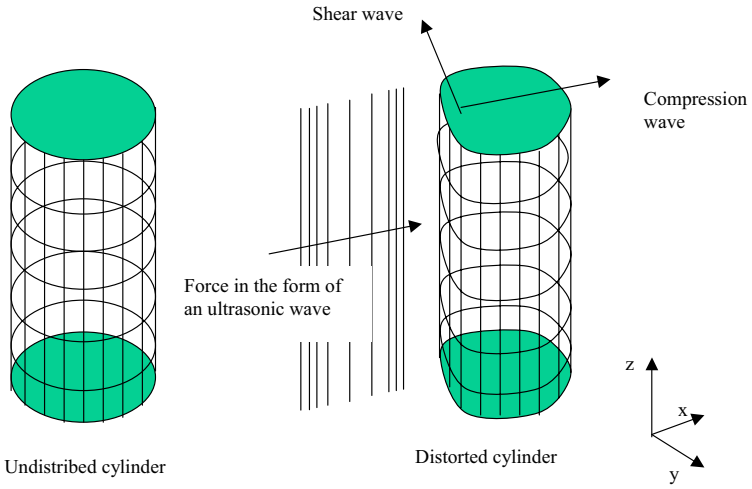

Figure 3.3: Cylinder excited by a force acting at a particular point in (x,y) and evenly in the z direction.

In a suspension, the wave travels from a fluid to either a solid or another fluid. As the wave hits the boundary of the two media part of the wave is reflected and part of the wave is transmitted. In the simple case of a plane wave arriving at a boundary that is perpendicular to the direction of the wave, calculating ratio of the intensity of the transmitted wave to the reflected wave is straight forward. This is done by considering the boundary condition at the interface and assuming the velocity and momentum to be continuous at this point. The result is that the amplitude of the wave being reflected depends on the difference in the characteristic impedances of the two media where the characteristic impedance is the product of the density by the velocity of the wave. Since we have considered a plane wave and a flat boundary, the only waves propagating are compression waves. The calculation is more elaborate if the wave progression is not perpendicular to the boundary and the interface on a solid. Details of this can be found in [14].

So, in short, the attenuation of the sound or ultrasound wave tells us something about

the nature of the medium the wave has passed through. If we now consider a sound wave travelling through a suspension of solid particles in a fluid, the attenuation of the sound wave will depend on the viscosity of the fluid, the bulk viscosity of the fluid, the difference in the characteristic impedance between the fluid and the solid i.e. differences in density and wave velocity in these two media, and finally the attenuation in the solid itself which is a function of loss tangent. Although this is not an exhaustive list it highlights the possibility of being able to estimate these parameters by measuring the attenuation of sound in a suspension of a solid in a fluid. Before going on to discuss the model, we must consider other effects that occur in a suspension, where we have two different media interacting.

3.1.1 Thermoelastic Scattering

Associated with a pressure wave of the ultrasound is a temperature wave, which is in phase with the pressure wave. This is depicted in the Figure 3.4, and shows an increase in temperature as the pressure increases during the compression part of the sound wave and decreasing again during the rarefraction part of the wave as the pressure decreases. In

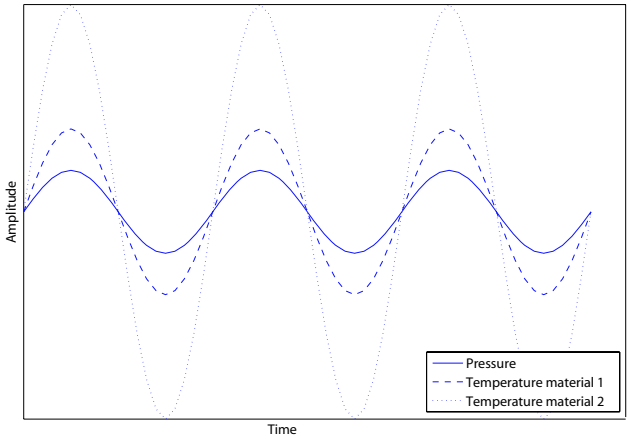

Figure 3.4: Plot of a Pressure wave with two temperature waves in different media

a suspension, there are two media that normally have different thermal properties. The result is that the temperature wave in the suspended particle is different in amplitude to that of the surrounding liquid. In order that there be no discontinuity at the boundary, heat flows into and out of the boundary layer to compensate for this difference in temperature. This causes the boundary layer to expand and contract and hence become the

source of a secondary wave (Figure 3.5). This is known as thermoelastic scattering. If we consider the particle to be spherical like or cylindrical, the effect, as viewed from a cross section through the cylinder or sphere, is of a symmetric monopole wave emanating from the scatterer. This wave decays quickly and is not noticable at a large distance from the

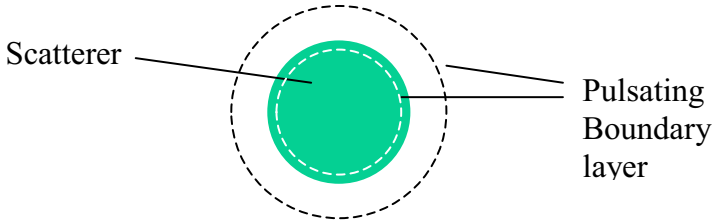

Figure 3.5: Diagram of an pulsating boundary layer, the source of a secondary sound wave.

scatterer. It does however dissipate energy and in some cases, such as for an emulsion of sunflower oil and water it can be the dominant effect in attenuation [16]. For fibres where the scatter diameter is close to the wavelength of the ultrasonic wave, this effect is small [17].

3.1.2 Viscous effects

In the previous section we discussed the attenuation and motion of a fluid not close to a boundary. We now consider the added effect of a boundary on a fluid. The added effect comes from the transverse motion the fluid is subjected to, due to the viscosity of the fluid and the proximity of a boundary. A description of this effect is given in [11]. The result is that the fluid has a secondary wave which is a function of the distance from the boundary

$$u' = ue^{-(1+1j)z/\delta} \tag{3.9}$$

$$\delta = \sqrt{2\eta/\rho_1\omega} \tag{3.10}$$

Where u' is the secondary wave, u is the primary wave, propagating parallel to the boundary, z is the distance perpendicular to boundary. The quantity δ is the viscous penetration depth or viscous skin depth. The effect of this viscous skin disappears as z increases until the resulting velocity is just that of the primary wave. At a large distance from the scatterer this wave is not noticeable, but as with the thermoelastic wave, it does dissipate energy at the boundary. The above expression is valid if the wavelength is much greater than the skin depth.

3.1.3 Other waves

In unbound solid, the wave progression can be described in terms of compression waves and shear waves. When a boundary is present additional constraints are place on the motion of an element in the medium. The results of these constraints are different propagation modes that depend not only on the elastic modulii but on the type and shape of the boundary. The following are some examples of these modes.

For a free cylinder excited so that a wave travels down its axis, it can produce torsional waves and flexural waves, as well as the compressional waves already discussed.

For a plate, the surface can exhibit Rayleigh waves, if the surface is free to move, or Stonely waves if the surface is constrained e.g. by a fluid, and Love waves. If a wave hits a boundary of a plate at a particular angle a creeping wave can be generated along the surface. If the plate is thin, Lamb waves can propagate. [18]

If the boundary is cylindrical, circumferential waves called whispering gallery can waves exist [19]. These are named after the effect they created in round buildings such as the dome of St. Paul Cathedral and are shown in Figure 3.6

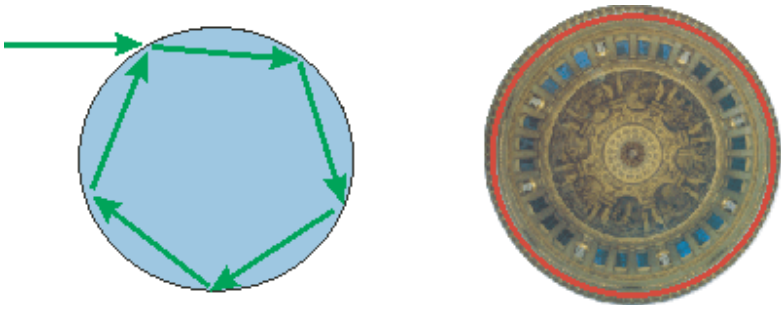

Figure 3.6: Whispering Gallery waves.

In the model that we present in the next section, these different modes are not considered per sae. But, the shear waves and the compression waves that are modelled, are subjected to the constraints of the boundaries. The effect on the velocity (or pressure) field is therefore the same if it is calculated using the modes listed above. However, the explanation for the behaviour, such as resonance is more difficult, if not impossible, unless we consider the modes described above.

3.1.4 Resonance

Resonance of a free cylinder occurs if the wavelength of a wave, or a multiple of wavelengths of a wave, travelling in the scatter matches the distance to one of the boundaries of the scatterer. If the wave is a compressional wave travelling down its axis then if a whole number of wavelengths fit into the length it will resonate. If a cylinder is excited

so that a wave travels down its axis, it can produce compressional waves, torsional waves and flexural waves. All of which can produce resonance effects. Further description of these phenomena is given in [11]

If a free cylinder is excited so that a compression wave travels in the radial direction, then resonance may occur if the wavelength matches the diameter. If we look at the case of a nylon fibre of diameter 55 μm, with a wave velocity of 2345 ms^{-1}, the frequency at which this would occur would be 42 MHz, from $f = c/\lambda$ (where λ is the wavelength and c is the wave velocity). This is much higher than the frequency range we are investigating. However, this type of excitation develops surface waves on the surface of the cylinder [20]. Since the path the wave is travelling is now equal to the circumference, $2\pi R$, the frequency at which resonance occurs is less than that of the compressional wave travelling radially. The waves that are excited are not just shear and compressional waves but are likely to be Rayleigh waves if the cylinder surface is free, and Stonely waves, if the cylinder is constrained, as when the cylinder is submersed in a fluid. In addition Whispering Gallery waves could also be generated.

Proof of the existence of these circumferential waves is given when the radius of the cylinder is large in comparison to the wavelength i.e. large values of ka where k is the wave number and a in this case is the radius [19]. But as yet we have no proof at lower values of ka. Thus, it is uncertain which type of wave is causing the resonance peaks in the nylon in the frequency range we are investigating. The resonance that is produced is a function of the frequency, wave velocity (both compressional and shear) and the radius of the cylinder. Since the cylinder is surrounded by water, the resonance is also a function of the ratio of the water density to the fibre density and to the velocity of the wave in water. This is discussed in more detail in Paper D. Further work is required to explore these resonance effects

We will now turn to examining the work that has been done in modelling these different phenomena in the scattering of ultrasound in suspensions before presenting an overview of the SCS model.

3.2 Historical Background

The propagation of sound in suspension has been discussed for at least a hundred years. Rayleigh [21] calculated the scattering effect of small spherical obstacles in a non-viscous atmosphere, when considering the effect on sound of fog and showed that the attenuation depends on the number of scattering particles and the ratio of their diameter to the wavelength of the sound. Knudsen [22] used expressions by Sewell in the calculation of attenuation for spherical and cylindrical particles in a viscous fluid to model audible sound in fog and smoke. Incidentally, Sewell's work confirmed the futility of using suspended or stretched wires for absorbing sound in rooms. In 1953, Epstein and Carhart [23] developed a model for the attenuation of sound by spherical particles where energy loss is due to the thermal and viscous losses in the boundary layer as well as scattering from the particle itself.

This model was modified slightly by Allegra and Hawley [24] and the resulting

Epstein-Carhart[23]/Allegra-Hawley [24] (ECAH) model has been the basis for investigations on attenuation and velocity measurements in emulsions [16]. A summary of different experiments on suspensions based on acoustic scattering theories is given in [25], though which specific model has been used in each case is not mentioned. In 1982, Habeger [17] derived a cylindrical version of ECAH model and tested this with experiments on suspensions of viscoelastic polymer fibres in water. The fibre parameters that were known or could be measured, using alternative methods, were used in the model with no adjustments. The values of the loss tangent and Poisson's ratio were set to fit the experimental data.

As the concentration increases, models relying on number of particles multiplied by the attenuation of a single scatterer start to become less appropriate. Multiple scattering models such as those developed by [26] have been developed for spherical particles but this cannot be directly applied to other shapes.

Another type of model that has actually been applied to paper pulp is Biot's model [27]. However, Habeger [17] claims that more difficulties lie in trying to assess the structural and material properties required in this model than in establishing the material properties in a scattering model.

Habeger [17] used the results of work on synthetic fibres to explain qualitatively the effect of the refining process on paper pulp using the results of ultrasound attenuation measurement and suggested more work was warranted [28]. The attenuation model used in this thesis is based on Habeger's model. To make the model more amenable to use in solving the inverse problem, where we estimate material properties from measurement of attenuation, an analytical solution for coefficients of expansion, B_n, was sought. This is derived in detail in Paper A. A general understanding of the model is presented in the next section.

3.3 Simple Cylinder Scattering (SCS) model

In the SCS model, we calculate the energy loss of an ultrasound wave after it has interacted with an infinitely long, cylindrical particle as depicted in Figure 3.7. The particle material is assumed to be viscoelastic and isotropic. To do this we need to establish the energy carried by the scattered wave. To simplify the problem, we split the velocity into two parts: one from the gradient of a scalar potential and the other from the curl of a vector potential. The first part represents a longitudinal wave and the second a transverse wave [15]. The problem is then solved in terms of these wave potentials. Hence if we wish to calculate the velocity then

$$V = \nabla\phi + \nabla \times A \tag{3.11}$$

Where ϕ is the scalar potential and A is the vector potential.

Normally a vector potential would require three scalar potentials to define it but in this case we define the vector potential as being transverse to the wave, hence we need only two scalar potentials. We take, as our starting point, the wave equation: one for the fluid and one for the solid. This relates the wave numbers to these scalar

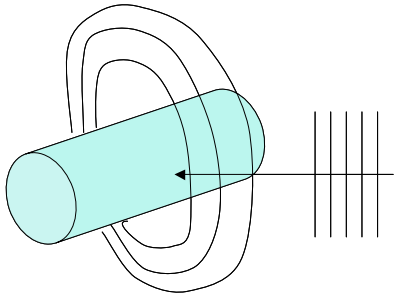

Figure 3.7: Diagram of an ultrasound plane wave being scattered off a cylindrical particle.

or wave potentials. The stress, strain and velocities can be expressed in terms of the wave potentials. These are divided into their cylindrical components, which make the boundary conditions simpler to apply. In the general case boundary conditions are that the velocities and the stresses in all three of the cylindrical co-ordinates are continuous across the solid/fluid interface.

However, before applying the boundary conditions, the wave potentials are expressed in terms of Bessel functions. Any function can be expressed as a series of Bessel function [29] so in general

$$f(z) = a_o J_o(z) + 2\sum_{n=1}^{\infty} a_n J_n(z). \tag{3.12}$$

Here the function $f(z)$ is expressed in a series of Bessel functions of the first order, $J_n(z)$ and unknown coefficients of expansion, a_n. In particular, the function $\exp(ir\cos\theta)$ [30] can be expressed as

$$e^{ir\cos\theta} = J_o(r) + 2\sum_{n=1}^{\infty} i^n J_n(r) cos(n\theta). \tag{3.13}$$

In cylindrical coordinates, r is the distance in the radial direction and θ is the angular distance. Hence solutions to the wave equation, when expressed in cylindrical co-ordinates, can be expressed in terms of Bessel functions. We continue therefore, by expanding the incident wave potential in the fluid and the wave potentials in the solid in terms of Bessel functions. The reflected wave potential in the fluid (and the shear waves potentials that exist in Habeger's model [17]) have to be expanded in terms of Bessel functions of the third order, often referred to as Hankel functions, as these potentials are not defined at the origin, i.e. do not span across $r = 0$. Because each order of the series is orthogonal, each of the n terms in the expansion can be treated separately. In this way we can solve the system of equations for the unknown coefficients of expansion.

The next part is to relate the coefficients of expansion to the energy loss of the incident wave as it interacts with a number of cylindrical scatterers. The average loss per unit

time due to the viscous and thermal processes has been showed by [23] to be equal to the product of the velocity and the stress integrated over the surface.

$$L = \frac{1}{2}\Re\left(\int V_j^* \tau_{ij} dS^i \right), \tag{3.14}$$

where L is the energy loss per unit time and length, V_j^* is the conjugate of the velocity, τ_{ij} is the stress.

If we assume we are at a large distance from the scatterer then these losses come down to the losses being a function of no other potentials but that of the reflected wave. This is shown in the expression for the energy loss L per unit time and per unit length by,

$$L = -\omega\rho_1 \sum_{n=0}^{\infty} \Re\left(\epsilon_n (B_n + B_n B_n^*)\right), \tag{3.15}$$

where $\epsilon_n = 1$ for $n = 0$, $\epsilon_n = 2$ for $n > 0$ and B_n are the coefficients of expansion. ρ_1 is the density of the water and ω is the angular frequency. $\Re$ indicates that only the real part is taken. To this we have to add the losses due to the scattering, which again, at a large distance from the scatterer come down to the losses being a function of no other potentials but that of the reflected wave,

$$L_s = \omega\rho_1 \sum_{n=0}^{\infty} \Re\left(\epsilon_n B_n B_n^*\right). \tag{3.16}$$

The total energy loss L_t is therefore the sum of 3.15 and 3.16,

$$L_t = -\omega\rho_1 \sum_{n=0}^{\infty} \Re\left(\epsilon_n B_n\right). \tag{3.17}$$

Since we know the mean energy flow is [23]

$$E = \frac{1}{2} k_{c_1} \omega \rho_1, \tag{3.18}$$

where k_{c_1} is the wave number of the compression wave in the fluid. Hence the attenuation due to a single scatterer is

$$\alpha = \frac{L_t}{E} = \frac{-2}{k_{c_1}} \sum_{n=0}^{\infty} \Re\left(B_n \epsilon_n\right). \tag{3.19}$$

Multiply this by the number of particles per unit length, N where

$$N = f_r/(\pi R^2) \tag{3.20}$$

and where f_r is the volume fraction, and R is the radius of the scatterer. We also take into account the fact that these fibres lie at different angles to the oncoming wave by

taking the average cosine of attenuation over the range of angles from 0° to 90°. The final expression is

$$\alpha = \frac{-2f_r}{\pi R^2 k_{c_1}} \Re \left(\int_0^{\frac{\pi}{2}} \epsilon_n B_n \cos(\psi) d\psi \right). \tag{3.21}$$

In this derivation an assumption is made in the step from equation (3.14) to equation (3.15) that the effect of viscosity of the water is negligible. More specifically,

$$\lim_{r\to\infty} \tau_{rr} = (i\omega\rho_1 - 2\eta k_{c_1}^2)(\phi_0 + \phi_r) - 2\eta(\phi_{0_1,rr} + \phi_{r_1,rr}) \tag{3.22}$$

to

$$\lim_{r\to\infty} \tau_{rr} \approx i\omega\rho_1(\phi_0 + \phi_r), \tag{3.23}$$

where τ_{rr} is the stress in the radial direction, η is the viscosity, ϕ_o is the incident wave potential, ϕ_r is the reflected wave potential and $\phi_{0_1,rr}$ and $\phi_{r_1,rr}$ are the gradients of the incident and reflective wave potentials along the r-axis in equation (3.22) respectively.

To account for this assumption the attenuation of water is added to the attenuation calculated in equation (3.21). This final expression is therefore,

$$\alpha = \frac{-2f_r}{\pi R^2 k_{c_1}} \Re \left(\int_0^{\frac{\pi}{2}} \epsilon_n B_n \cos(\psi) d\psi \right) + \alpha_w, \tag{3.24}$$

where α_w is the attenuation due to water.

In addition to being able to calculate the attenuation, from the coefficients of expansions we can also calculate the wave potentials in the area surrounding a single fibre. The resulting wave potential from a single fibre is shown in Figure 3.8. To clarify the effect of the fibre on the reflected field potential the same plot is drawn but this time with the incident wave potential removed in Figure 3.9.

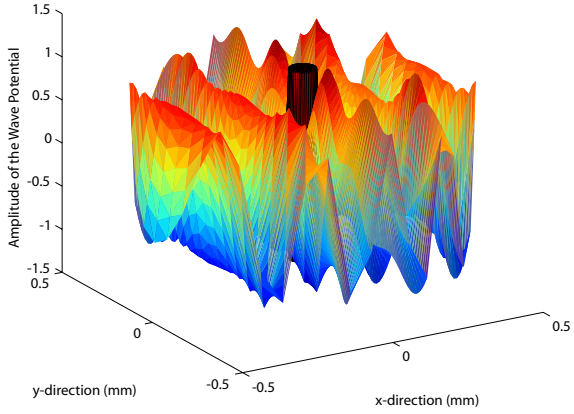

Figure 3.8: Amplitude of the wave potential surrounding a fibre scattering an plane ultrasonic wave.

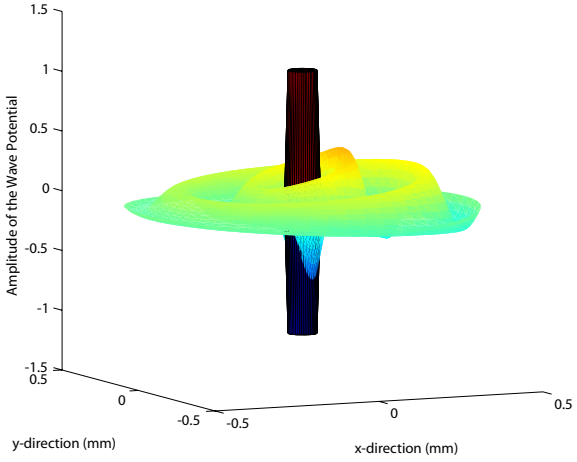

Figure 3.9: Amplitude of the reflected wave potential surrounding a fibre scattering an plane ultrasonic wave.

Chapter 4

Summary of the Papers

4.1 Paper A - Estimating Suspended Fibre Material Properties by Modelling Ultrasound Attenuation

Authors: Yvonne Aitomäki and Torbjörn Löfqvist
Reproduced from: Proceedings of International Conference 'Mathmatical Modelling of Wave Phenomena 2005´

Summary
The SCS model is described in detail. This is compared to the model that includes thermal and viscous shear effects in the fluid derived by Habeger [17]. Experimental derived attenuation for a suspension of nylon fibres cut from fishing line in water is compared to the predicted attenuation from the model results. The nylon used in the fishing line is a polyamide copolymer so the exact material properties of the fibre were difficult to establish since the type of the copolymer was not known. The results lay between those expected for nylon 66 and nylon 6. Resonance peaks in the attenuation were both predicted and found experimentally. The conclusion was that it appears the model is sufficiently sensitive to material properties that estimation of these properties from the attenuation may be possible.

4.2 Paper B -Ultrasonic Measurements and Modelling of Attenuation and Phase Velocity in Pulp Suspensions

Authors: Jan Niemi, Yvonne Aitomäki and Torbjörn Löfqvist
Reproduced from: Proceeding of IEEE Ultrasonic Symposium, Rotterdam, Holland 2005

Summary
This paper introduces a method of performing phase unwrapping that minimises discontinuities in the phase shift. This is used to calculate the phase velocity in pulps of different consistency. The results show that dispersion is caused by fibres and correlates with mass fraction. Attenuation measurements of pulp are also made, with the aim of finding resonance peaks in the frequency response of the attenuation predicted by the model. Clear peaks are not found. This is thought to be due to the affect of the distributed diameters of the pulp fibres. Estimations of the properties are made from these curves but comparison with known values was not done. This is due to the difficulties in carrying out single fibre tests on saturated wood fibres.
Personal contribution
Work based on the attenuation was carried out by myself. The phase velocity work was carried out by Jan Niemi.

4.3 Paper C -Inverse Estimation of Material Properties from Ultrasound Attenuation in Fibre suspensions

Authors: Yvonne Aitomäki and Torbjörn Löfqvist
To be submitted to: Elsevier Ultrasonics

Summary
In this paper experiments on nylon 66 give evidence for the effect that different diameter have on the attenuation. This supports the SCS model. An optimisation procedure is implemented to estimate the accuracy with which material parameter can be estimated from the model. The results show that the shear modulus is within expected range. Density measurement are overestimated by 10%-15%. However, Poisson's ratio is overestimated and consequently underestimates the value of Young's Modulus. The suggested reason for this is that the model underestimates of the attenuation at high frequencies. This could be caused by additional attenuation effects that have not been taken into account by the model or due to the anisotropic nature of the fibres.

4.4 Paper D - Sounding Out Paper Pulp: Ultrasound Spectroscopy of Dilute Viscoelastic Fibre Suspensions

Authors: Yvonne Aitomäki and Torbjörn Löfqvist
Submitted to: Acoustics and ultrasonics in the processing of industrial soft solids

Summary
The reason why the resonance peaks appear in the frequency response of the attenuation is explored in this paper. We show here that the resonance of the first peaks is connected to the shear wave velocity in the fibre and its diameter. Hence experimentally determining the location of the first resonance peak will help establish the value of the shear modulus. This backs up the results in Paper C, which showed that the shear modulus was estimated to within a previously established range. The reason that the first resonance peaks are associated with shear waves is because the shear waves has a lower velocity than the compression wave. The exact nature of the wave that causes this resonance is not yet established, since the proof that they are Rayleigh waves relies on asymptotic values for the Bessel functions, which are only valid for ka (the product of the radius and the wave number) values much greater than one. Since this is not the case with the fibre suspension used, we cannot draw the same conclusion that the peaks in attenuation are also caused by Rayleigh waves.

Chapter 5

Discussion

Some issues are raised in the papers on the reliability of the experimental measurements and the accuracy of the model. We take the opportunity now, to discuss these in more detail here.

The temperature dependency of attenuation of water has not been addressed in these papers. However, data from [31] shows the effect of attenuation on water and is plotted below.

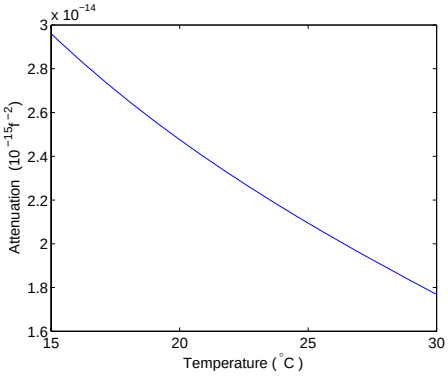

Figure 5.1: Temperature dependence of Attenuation per frequency squared [31]

Using this data and the temperature of the suspension used in Paper C that gives the maximum attenuation difference, the error in the attenuation is estimated at 6%. Temperature adjustment will be made in future experiments.

The results of the parameter estimation in Paper C showed that the compression wave velocity in the fibre is overestimated. This could be because the model underestimates the attenuation. One way of increasing the theoretical attenuation at high frequencies

without moving the peak due to the shear velocity, and consequently the shear modulus and density, is to assume a higher value of Poisson's ratio. This increases the compressional wave velocity. This is shown in Figure 5.2 where the best-fit line is taken from that of the 55 μm fibre used in the experiments described in Paper C. For this plot, Poisson's ratio was estimated at 0.49, and compared to a theoretical attenuation calculated using Poisson's ratio of 0.42. As can be seen, the attenuation is lower. Hence the most likely explanation for this overestimation of the velocity is that the model underestimates the attenuation at high frequencies, which causes the parameter optimisation process to increase the value of Poisson's ratio, and hence the compressional wave speed, when matching the theoretical and experimental attenuation.

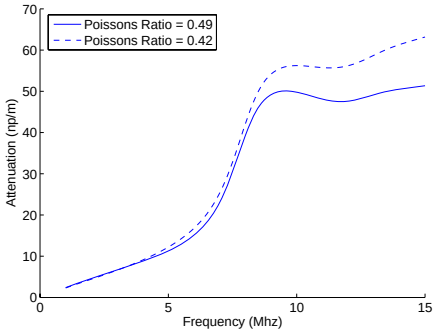

Figure 5.2: Effect of reducing Poisson's ratio on the Attenuation [31]

One possible reason for the lower prediction of attenuation at higher frequencies is the effect of neglecting multiple scattering effects. Multiple scattering is where the wave interacts with more than one scatterer. Although multiple scattering theories exist, they have only been developed for spherical particles so far [26]. A possible way of approximating this effect is to assume that the next interaction is the same as if it were the first interaction. But, that in addition we add the intrinsic attenuation of the wave travelling through a solid. An approximation for the attenuation in a solid have been given earlier in equation (3.5). So, the complete theoretical attenuation becomes:

$$\alpha_t = \alpha + (1 - f_r)\alpha_w + f_r\alpha_f \tag{5.1}$$

where α is the attenuation calculated from the SCS model presented in equation 3.21, α_w is the attenuation of water and α_f is the attenuation in the solid.

Further investigations using this modification will be carried out to see if it improves the predicted attenuation at higher frequencies.

The effect of temperature on the attenuation in water, neglecting thermal effects and transverse waves in the water all affect the level of the attenuation but should not significantly affect the shape of the attenuation curve over this frequency range. Thus

these factors could be ignored if comparative measures are required or compensation made for them. However, the consequence of the possible multiple scattering effects will affect the shape of the attenuation curve and this leads to more unpredictable errors in the estimation of the parameters.

Chapter 6

Conclusion

As far as online paper pulp quality measurement goes, we have established that we can estimated shear modulus and to a certain extent density, from nylon 66 fibres in suspension (Paper A & C). But more importantly, we propose that the frequency range that should be used is in the region where the wavelength is of the order of the radius (Paper C & D). Some initial trials have been done on pulps which have highlighted the problem of non-uniformity of radius of the fibres and the difficulty with assessing the accuracy of these measurements (Paper B).

When solving inverse problems, one is always faced with the fact that the result could be caused by a number of different inputs. The more information one has, the better the chances of finding an accurate estimation of these inputs. In our application the result is the attenuation measurement and the inputs are the material properties. In looking at higher frequencies where the wavelength is comparable to the size of the scatterer, we may be introducing errors into the model, as effects that have not been accounted for affect the accuracy, but in increasing the frequency range we also obtain more information about the material properties. The key is then to find the right balance.

For the method as it is to have application in the paper and pulp industry there are certain conditions that need to be fulfilled. These are that we find peaks in the frequency response of the attenuation in pulp, know the diameter distribution of the fibres and the hollow nature of the fibres does not significantly alter the results. We can then, potentially, be able to establish the shear modulus of the pulp fibres. If the shear modulus is a factor in paper quality, we may be nearer than we think to the online measurement of paper pulp quality using ultrasonic spectroscopy. Improving the model may allow us to estimate further properties and take into account the fibres being hollow.

Chapter 7

Further Work

7.1 Getting this to work

The aim of these studies is to develop an online fibre characterization measurement method for use in the paper and pulp industry. Questions that we have to address to take this project further are:

- Is this model adequate for modelling hollow fibres?
- Does work for different materials?
- How accurate is the parameter estimation for other materials?
- How do we deal with non-uniform diameters?
- Can we get more data to improve the parameter estimation?

Is this model adequate for modelling hollow fibres?

Models are available for layered cylinders [32]. However, the set of equations to solve is larger and another parameter is required to be estimated but, due to the slip boundary condition used, the equations are not as involved as the set used in the SCS model. As a first step we can experiment on hollow and solid synthetic fibres to assess the effect this has on attenuation. Using the layered model we could also predict the differences. If the model predicts the attenuation better than the SCS model then this could be used in place the SCS model in the parameter estimation procedure.

Does work for different materials?

To establish the reliability of the estimation of material properties different types of fibre should be tested. The plan is to continue to test with rayon and polyester fibres.

We also intend to work with pulp testing laboratories in an effort to gain more accurate knowledge of the material properties of pulp fibres in suspension. Of particular interest is the variability from one pulp to another and the degree of accuracy required by the pulp manufactures for the parameter estimation to be useful in controlling pulp or paper production.

How do we deal with non-uniform fibres?

Pulp fibres differ considerably from one other. They have different diameters, thicknesses, and elasticity. However, their density does not vary much. The different densities of the fibres come from differences in the wall thickness. If data is available on the fibre wall thickness and the diameter, it might be possible to estimate fibre properties as was done in Paper B. However, it seems unlikely that both diameter and material properties could both be estimated. This depends considerably on the variation in the pulp fibres. Different sizes should produce peaks at different frequencies. This may provide a good means of differentiating between the type of fibre in the pulp. However, large fibres may have different properties from smaller fibres and will consequently add further ambiguity in solving the inverse problem.

Can we get more data to improve the parameter estimation?

In inverse problems, the more data there is available the less ambiguous the solution. Hence we need to search for ways of obtaining more data.

Increasing the frequency range

Increasing the frequency range increases the spectra available for the estimation process. From Paper C, the suggestion is to aim for frequencies where at least the first resonance peak is available. Since pulp fibres have average diameters of 30 to 40 microns as opposed to 50 to 55 microns of the nylon, the frequency range could be increased to investigate whether resonance peaks exist beyond the range we are currently using.

Investigating the possibility of modelling to measure phase

In [33], the coefficient of expansion of the reflected wave from which the attenuation is derived is expressed in terms of a phase shift. Using this model we can model both the phase velocity shift and attenuation and hence take two measurements to fit both sets to the data.

Will laser excitation provide us with more information?

Work is currently being done using photoacoustics to characterise paper pulp. It may be possible that this would provide additional information on the pulp fibres such as the volume fraction, or even their diameters, that can be used to improve the estimation of the material properties.

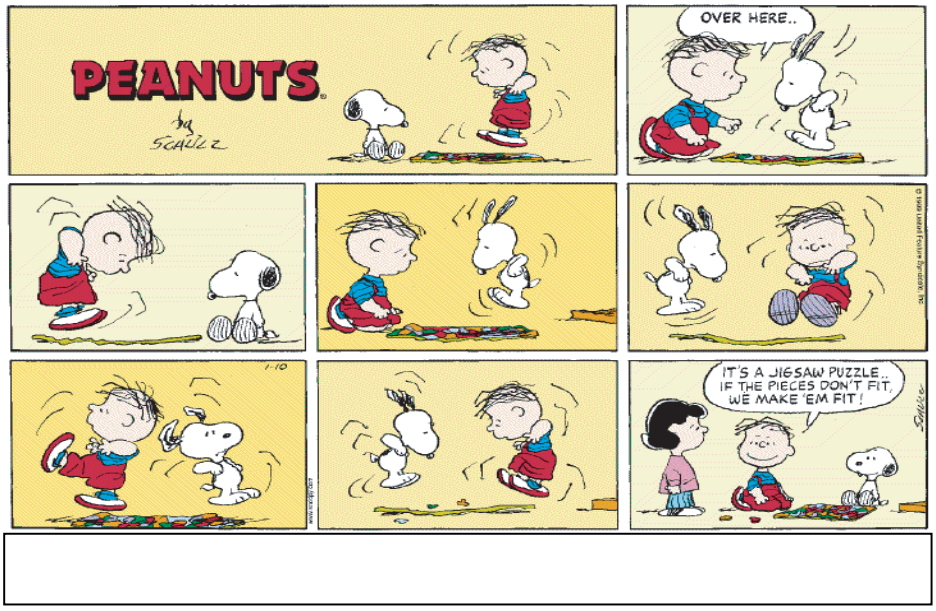

Figure 7.1: Solving the Inverse Problem

References

[1] "Swedish foresty agency international statistics." http://www.svo.se/minskog/ Templates/EPFileListing.asp?id=16698, 2006-03-04.

[2] J. Levlin and L. Söderhjelm, *Pulp and Paper Testing*. Fapet Oy, 1999.

[3] P. Brodeur and J. Gerhardstein, "Overview of applications of ultrasonics in the pulp and paper industry," in *1998 IEEE Ultrasonics Symposium*, pp. 809–815, 1998.

[4] Salesperson, "Lorentzen-wettre personal communication," April 2006.

[5] K. K. Piteå, *Välkommen till en rundvandring in Kappa Kraftliner Piteå*. 2006.

[6] T. Wikström, *Flow and rheology of pulp suspensions at medium consistency*. Phd thesis, Chalmers University of Technology, 2002.

[7] M. Jansson, "Stfi-packforsk personal communication," Feb 2006.

[8] M. Jansson and A. Jacobs, "Recycling fibres undergo fibre wall analysis," *Beyond*, no. 1, p. 4, 2006.

[9] H. Karlsson and P. Fransson, "Stfi fibermaster fives the papermaker new muscles," *Sv. Papperstidning*, vol. 10, no. 26, 97.

[10] E. Ehrnrooth, *Softening and mechanical behaviour of single wood pulp fibres - the influence of matrix composition and chemical and physical characteristics*. Phd thesis, Department of Wood and Polymer Chemistry, University of Helsinki, 1982.

[11] L. Kinsler, A. Frey, A. Coppens, and J. Sanders, *Fundamentals of Acoustics*. John Wiley and Sons Inc., 4 ed. ed., 2000.

[12] Kolsky, *Stress Waves in Solids*, ch. V, p. 118. Dover, 1963.

[13] A. Bhatia, *Ultrasonic Absorption*, ch. 11, p. 272. Dover, 1968.

[14] Kolsky, *Stress Waves in Solids*. Dover, 1963.

[15] P. Morse and H. Feshbach, *Method of Theoretical Physics*, vol. II, ch. 13. McGraw-Hill Book Company, Inc, 1953.

[16] D. McClements and M. Povey, "Scattering of ultrasound by emulsions," *Journal of Physics D: Applied Physics*, vol. 22, pp. 38–47, 1989.

[17] C. Habeger, "The attenuation of ultrsound in dilute polymeric fiber suspensions," *Journal of Acoustical Society of America*, vol. 72, pp. 870–878, sep 1982.

[18] Y. Fung, *Foundations of Solid Mechanics*. Prentice-Hall, 1965.

[19] J. Dickey, G. Frisk, and H. Uberall, "Whispering gallery wave modes on elastic cylinders," *Journal of the Acoustical Society of America*, vol. 59, pp. 1339–1346, June 1976.

[20] R. Doolittle, H. Uberall, and P. Ugincius, "Sound scattering by elastic cylinders," *Journal of the Acoustical Society of America*, vol. 43, no. 1, pp. 1–14, 1968.

[21] Rayleigh, *The Theory of Sound*. Macmillan, 1926.

[22] V. Knudsen, J. Wilson, and N. Anderson, "The attenuation of audible sound in fog and smoke," *The Journal fo the Acoustical Society of America*, vol. 20, pp. 849–857, Nov 1948.

[23] P. Epstein and R. Carhart, "The absorption of sound in syspensions and emulsions. i. water fog in air," *The Journal of the Acoustical Society of America*, vol. 25, pp. 553–565, May 1953.

[24] J. Allegra and S. Hawley, "Attenation of sound in suspension and emulsions: Theory and experiments," *The Journal of the Acoustical Society of America*, vol. 51, pp. 1545–1564, 2 1972.

[25] M. Povey, *Ultrasonic Techniques for Fluid Characterization*, ch. A.4, p. 179. Academic Press, 1997.

[26] P. Lloyd and M. Berry, "Wave propagations through an assembly of spheres iv. relations between different multiple scattering theories," *Proc. Phys. Soc.*, vol. 91, pp. 678–688, 1967.

[27] D. Adams, *Ultrasonic transmission through paper fiber suspensions*. PhD thesis, University of London, 1975.

[28] C. Habeger and G. Baum, "Ultrasonic characterizations of fibre suspension," IPC Technical Paper series 118, The Institue of Paper Chemistry, Appleton, Wisconsin, Nov 1981.

[29] M. Abramowitza and I. Stegun, *Handbook of mathematical functions*. Dover, 1972.

[30] M. Morse, P and K. Ingard, *Theoretical Acoustics*, ch. 8, p. 401. Princetown University Press, 1986.

[31] F. Fisher and V. Simmons, "Sound absorption in sea water," *Journal of the Acoustical Society of America*, vol. 62, pp. 558–564, Sept 77.

[32] L. Flax and N. W., "Acoustic reflection from layered elastic absorptive cylinders," *Journal of the Acoustical Society of America*, vol. 61, pp. 307–312, Feb 1977.

[33] J. Faran, "Sound scattering by solid cylinders and spheres," *Journal of the Acoustical Society of America*, vol. 23, pp. 405–418, July 1951.

Part II

Paper A

Estimating Suspended Fibre Material Properties by Modelling Ultrasound Attenuation

Authors:
Yvonne Aitomäki and Torbjörn Löfqvist

Reformatted version of paper originally published in:
Proceedings of International Conference 'Mathmatical Modelling of Wave Phenomena 2005´

Estimating Suspended Fibre Material Properties by modelling Ultrasound Attenuation

Yvonne Aitomäki and Torbjörn Löfqvist

Abstract

An analytical model for use in the inverse problem of estimating material properties of suspended fibres from ultrasonic attenuation has been developed. The ultrasound attenuation is derived theoretically from the energy losses arising when a plane wave is scattered and absorbed off an infinitely long, isotropic, viscoelastic cylinder. By neglecting thermal considerations and assuming low viscosity in the suspending fluid, we can make additional assumptions that provide us with a tractable set of equations that can be solved analytically. The model can then be to used in inverse methods of estimating material properties. We verify the model with experimentally obtained values of attenuation for saturated Nylon fibres. The experimental results from Nylon fibres show local peaks in the attenuation which are thought to be due to the resonant absorption at the eigenfrequencies of the fibres. The results of the experiments show that the model is sufficiently sensitive to detect differences in different types of Nylon. Applications for suspended fibre characterization can be found in the paper manufacturing industry.

List of Symbols

Unless otherwise indicated subscript 1 refers to the fluid medium and subscript 2 refers to the solid medium.

$\mathbf{A_1}$,$\mathbf{A_2}$	transverse vector potentials	$\mathbf{M}, \mathbf{N}$	transverse vector potential
a_c	$R \times k_c$	M	elastic modulus
a_s	$R \times k_s$	R	radius of the fibre
a_{cc}	$R \times k_{cc}$	r , θ, z	cylindrical coordinates
a_{sc}	$R \times k_{sc}$	V	velocity
a_{cs}	$R \times k_{cs}$	α	acoustic attenuation
B_n, D_n, E_n	coefficients of expansion	α_1	acoustic attenuation ín water
C_p	heat capacity in the fluid	β	thermal expansivity
c	velocity of sound	$\tan\delta_2$	loss tangent of the viscoelastic solid
$\mathbf{c}$	complex speed of sound in the sound	ϵ_{ij}	strain
f_r	volume fraction of fibres	η_1	viscosity of the fluid
$H_n^{(1)}$	nth order Hankel function of the first kind	Γ_{ij}^l	Christoffel symbol
J_n	nth order Bessel function of the first kind	λ	wavelength
K	heat conductivity coefficient	ω	angular frequency

$\hat{\mathbf{k}}$	unit vector along the z-axis in cylindrical co-ordinates	ρ	density
		λ_2, μ_2	Lamê's 1st and 2nd constants
k_c	wave number of the compressional wave	υ_2	Poisson's ratio
k_s	wave number of the transverse wave	ψ	the angle between the incident wave and the longitudinal axis of the cylinder
k_{cc}	wave number of the compressional wave along the r-axis	ϕ_c	compressional wave scalar potential
k_{cs}	wave number component of the compressional wave along the z-axis	ϕ_o	incident compressional wave scalar potential
k_{sc}	wave numbers of the transverse wave along the r-axis	ϕ_r	reflected compressional wave scalar potential
		χ, ξ	transverse wave scalar potentials

1 Introduction

Our research is aimed at the on-line estimation of the characteristics of pulp fibres suspended in water. An application is in the paper manufacturing industry where estimating fibre characteristics can potentially improve the quality control of the finished paper. The measurement method used is based on ultrasound as it is rapid, inexpensive, non-destructive and non-intrusive.

The focus of our investigation is on establishing the material properties of the suspended, fluid-saturated fibres from ultrasonic attenuation measurements. To do this we need to solve the inverse problem of deriving these properties from the attenuation. We therefore require a model that relates attenuation to material properties and one that is analytical since this is more amenable than numerical solutions for solving the inverse problem. Habeger established a model related attenuation to material properties, where the equations are solved numerically [1]. We have developed an analytical solution based on the same equations.

Habeger's model is a cylindrical extension of the Epstein-Carhart [2]/Allegra-Hawley [3] model. In the calculation of attenuation, the set of equations are solved numerically and are based on a number of different material properties. By neglecting thermal effects and assuming low viscosity in the suspending fluid, we can make additional assumptions that provide us with a more tractable set of equations that can then be solved analytically.

In this paper we describe the simplified model used to relate the attenuation to the material properties of the fluid saturated fibres. We compare the analytical solution with that obtained by a numerical solution of the non-simplified equation system [1], to verify the validity of the additional assumptions that are made. We then verify the model with experimentally obtained values of attenuation for saturated Nylon fibres. We go on to discuss the results, draw conclusions and outline the next steps in our investigations.

2 Theory

The attenuation is derived from calculating the energy losses arising when a plane wave is incident upon an infinitely long, straight cylinder. The cylinder material is assumed to be isotropic and viscoelastic. The energy losses taken into account are from the wave being partially reflected, partially transmitted at the solid/fluid interface and from the generation of damped, transverse waves in the solid medium at the boundary. The highly damped thermal skin layer, that is generated by the acoustically induced pulsations of the solid is shown by [1] to have the greatest effect where the thermal wavelength is of the order of the radius. We, therefore, consider frequencies above this region and hence the thermal effects are neglected in the derivation of attenuation. The advantage is that the thermal material properties of the fibre and fluid can then be neglected, reducing the number of material properties in the solution and hence increasing the feasibility of estimating the remaining material properties from attenuation measurements. A viscous wave in the fluid (as defined by [2]) is also generated but again this is highly damped and is neglected in the final stages of the derivation.

Expressions for the wave potentials from the conservation of mass, energy and momentum were derived by [2] and are expressed for the fluid as:

$$\nabla \cdot \mathbf{A_1} = 0 \tag{1}$$

$$\nabla^2 \phi_{c_1} = -k_{c_1}^2 \phi_{c_1} \tag{2}$$

$$\nabla \times \nabla \times \mathbf{A_1} = k_{s_1}^2 \mathbf{A_1} \tag{3}$$

$$\mathbf{V_1} = -\nabla \phi_{c_1} + \nabla \times \mathbf{A_1} \tag{4}$$

where, $k_{c_1} = \omega / c_1$ and $k_{s_1} = \sqrt{i\omega\rho_1/\eta_1}$.

In the solid, the displacement potentials are used instead of the velocity potentials. Hence,

$$\nabla \cdot \mathbf{A_2} = 0 \tag{5}$$

$$\nabla^2 \phi_{c_2} = -k_{c_2}^2 \phi_{c_2} \tag{6}$$

$$\nabla \times \nabla \times \mathbf{A_2} = k_{s_2}^2 \mathbf{A_2} \tag{7}$$

$$\mathbf{V_2} = i\omega \left(\nabla \phi_{c_2} - \nabla \times \mathbf{A_2} \right) \tag{8}$$

where $k_{c_2} = \omega / (c_2(1 - i \tan \delta_2/2))$ and $k_{s_2} = \sqrt{i\omega\rho_2/\mu_2}$. Further details of the definition for the wave number in a viscoelastic solid and the complex shear modulus, μ_2, are described in the Appendix.

The stress tensor can be expressed in terms of the wave potentials:

$$\tau_{ij_1} = \eta_1 \left[(k_{s_1}^2 - 2k_{c_1}^2) \phi_{c_1} \right] \delta_{ij} + 2\eta_1 \dot{\epsilon}_{ij} \tag{9}$$

$$\tau_{ij_2} = \left[(\omega^2 \rho_2 - 2\mu_2 k_{c_2}^2) \phi_{c_2} \right] \delta_{ij} + 2\mu_2 \epsilon_{ij} \tag{10}$$

Where the strain is

$$\epsilon_{ij} = \frac{1}{2}(V_{i,j} + V_{j,i} - 2\Gamma^l_{ij}V_l) \tag{11}$$

The fluid wave potential is divided into an incident part and a reflected part, $\phi_{c_1} = \phi_{o_1} + \phi_{r_1}$. The incident plane wave potential, ϕ_{o_1}, is expressed in cylindrical coordinates and we let this equal $e^{i(k_{cc_1}r + k_{cs_1}z - \omega t)}$ as in [1].

Since the plane of the cylinder lies at an angle ψ to the incident wave, the wave numbers are expressed in terms of their components along the cylindrical coordinate axes.

$$k_{cc_1} = k_{c_1}\cos(\psi) \tag{12}$$

$$k_{cs_1} = k_{c_1}\sin(\psi) \tag{13}$$

The inicident wave potential is expanded using Bessel functions of the first kind [4] as

$$\phi_{o_1} = \left(J_0(k_{cc_1}r) + 2\sum_{n=1}^{\infty} i^n \cos n\theta J_n(k_{cc_1}r)\right) e^{i(k_{cs_1}z - \omega t)} \tag{14}$$

And the reflected wave potential in the fluid expanded using Hankel functions of the first kind:

$$\phi_{r_1} = \left(B_{0_1}H_0^{(1)}(k_{cc_1}r) + 2\sum_{n=1}^{\infty} i^n \cos n\theta B_{n_1}H_n^{(1)}(k_{cc_1}r)\right) e^{i(k_{cs_1}z - \omega t)} \tag{15}$$

The combination of the equations (14) and (15) give us an expression for ϕ_{o_1} expanded in terms of Bessel and Hankel functions. To meet the boundary conditions for all values of z and t, the time and z dependence of the potentials must be the same as ϕ_{o_1}. The equivalent expression for the compressional wave potential in the solid is

$$\phi_{c_2} = \left(B_{0_2}J_0(k_{cc_2}r) + 2\sum_{n=1}^{\infty} i^n \cos n\theta B_{n_2}J_n(k_{cc_2}r)\right) e^{i(k_{cs_1}z - \omega t)} \tag{16}$$

where, $k_{cc_2} = \sqrt{(k_{c_2}^2 - k_{cs_1}^2)}$.

To meet the boundary conditions in cylindrical coordinates, the transverse potential can be expanded in terms of two independent scalar potentials, see [5] such that, $\mathbf{M} = \nabla \times \chi\hat{\mathbf{k}}$, $\mathbf{N} = \nabla \times \nabla \times \xi\hat{\mathbf{k}}$ and $\mathbf{A} = \mathbf{M} + \mathbf{N}$. Where χ and ξ are solutions to the scalar Helmholtz equation so, $\nabla^2\chi = -k_{s_2}^2\chi$ and $\nabla^2\xi = -k_{s_2}^2\xi$. The energy dissipated by the transverse waves in the fluid are however very small when the viscosity is low hence these are neglected. Expanding the transverse waves in solid in terms of Bessel and Hankel functions we get

$$k_{s_2}^2\xi_2 = \left(D_{0_2}J_0(k_{sc_2}r) + 2\sum_{n=1}^{\infty} i^n \frac{\partial \cos n\theta}{\partial\theta} D_{n_2}J_n(k_{sc_2}r)\right) e^{i(k_{cs_1}z - \omega t)} \tag{17}$$

$$ik_{cs_1}\chi_2 = \left(E_{0_2}J_0(k_{sc_2}r) + 2\sum_{n=1}^{\infty} i^n \cos n\theta E_{n_2}J_n(k_{sc_2}r)\right) e^{i(k_{cs_1}z - \omega t)} \tag{18}$$

where, $k_{sc_2} = \sqrt{k_{s_2}^2 - k_{cs_2}^2}$.

The boundary conditions are that the velocity along the surface normal and the stresses in all directions are continuous at the solid-fluid interface. So at $r = R_2$, $V_{r_1} = V_{r_2}$, $\tau_{rr_1} = \tau_{rr_2}$, $\tau_{r\theta_1} = \tau_{r\theta_2}$ and $\tau_{rz_1} = \tau_{rz_2}$. Since we neglect the velocity of the viscous wave in the fluid we do not consider the boundary conditions of continuous velocity at the solid/fluid interface in the θ and z directions. The boundary conditions are expressed in terms of the potentials using (4), (8) and (9)-(11) and then expanded according to (14)-(18). The angular dependencies of the functions are orthogonal so the coefficients can be determined by applying the boundary condition to each order of expansion separately.

For $n \neq 0$,

$$a_{cc_1}J'(a_{cc_1}) + B_{n_1}a_{cc_1}H_n^{(1)\prime}(a_{cc_1}) = -i\omega\big[B_{n_2}a_{cc_2}J_n'(a_{cc_2}) - E_{n_2}a_{sc_2}J_n'(a_{sc_2}) + n^2D_{n_2}J_n(a_{sc_2})\big] \quad (19)$$

$$\eta_1\big\{[(a_{s_1}^2 - 2a_{c_1}^2)J_n(a_{cc_1}) - 2a_{cc_1}^2J_n''(a_{cc_1})] + B_{n_1}[(a_{s_1}^2 - 2a_{c_1}^2)H_n^{(1)}(a_{cc_1}) - 2a_{cc_1}^2H_n^{(1)\prime\prime}(a_{cc_1})]\big\} = \mu_2\big\{B_{n_2}[(a_{s_2}^2 - 2a_{c_2}^2)J_n(a_{cc_2}) - 2a_{cc_2}^2J_n''(a_{cc_2})] + 2D_{n_2}n^2[J_n(a_{sc_2}) - a_{sc_2}J_n'(a_{sc_2})] + 2E_{n_2}a_{sc_2}^2J_n''(a_{sc_2})\big\} \quad (20)$$

$$\eta_1\big\{a_{cc_1}J_n'(a_{cc_1}) - J_n(a_{cc_1}) + B_{n_1}[a_{cc_1}H_n^{(1)\prime}(a_{cc_1}) - H_n^{(1)}(a_{cc_1})]\big\} = \mu_2\big\{B_{n_2}[a_{cc_2}J_n'(a_{cc_2}) - J_n(a_{cc_2})] + \frac{1}{2}D_{n_2}[n^2J_n(a_{sc_2}) - a_{sc_2}J_n'(a_{sc_2}) + a_{sc_2}^2J_n''(a_{sc_2})] + E_{n_2}[J_n(a_{sc_2}) - a_{sc_2}J_n'(a_{sc_2})]\big\} \quad (21)$$

$$\eta_1\big\{2a_{cs_1}[a_{cc_1}J_n'(a_{cc_1}) + a_{cc_1}B_{n_1}H_n^{(1)\prime}(a_{cc_1})]\big\} = \mu_2\big\{2a_{cs_1}a_{cc_2}B_{n_2}J_n'(a_{cc_2}) + D_{n_2}n^2a_{cs_1}J_n(a_{sc_2}) + E_{n_2}a_{sc_2}J_n'(a_{sc_2})\frac{(a_{sc_2}^2 - a_{cs_1}^2)}{a_{cs_1}}\big\} \quad (22)$$

For $n = 0$, D_{n_2} is only present (21) hence the solution in this case is that $D_{n_2} = 0$. Hence for $n = 0$ there are 3 equations and 3 unknowns and for $n \neq 0$ there are 4 equations and 4 unknowns. The expression for the coefficients $B_{n_1}, B_{n_2}, D_{n_2}, E_{n_2}$ was then found for $n = 0$ and $n \neq 0$ using Maple ©,Maplesoft, Waterloo, Canada.

This gives us the solution to the conservation equations. The subsequent derivation of the loss in energy due to the the scattering and absorption by the cylinder follows that of [1]. The resulting expression for the attenuation, α is:

$$\alpha = \frac{-2f_r}{\pi R^2 k_{c_1}}\Re\left(\int_0^{\frac{\pi}{2}}\cos(\psi)(B_{0_1} + 2B_{1_1} + 2B_{2_1})d\psi\right) \quad (23)$$

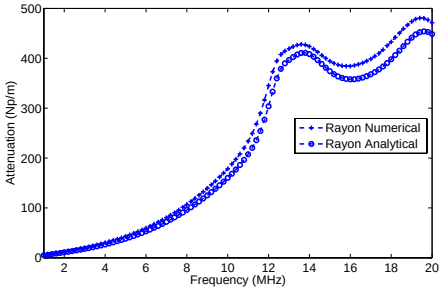

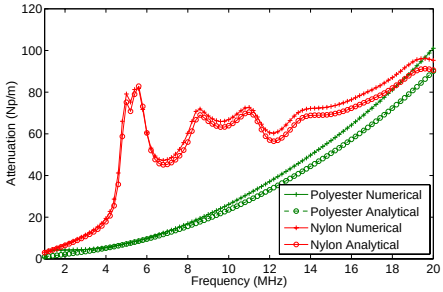

Figure 1: test

Figure 2: Attenuation as a function of frequency for different fibres. The attenuation is expressed in nepers per meter (Np/m),where neper (Np) is a dimensionless unit [6]. $\eta_1 = 9.4 \times 10^{-4}\, Nsm^{-2}$, $\rho_1 = 996\, kgm^{-3}$, $c_1 = 1490\, ms^{-1}$, $K_1 = 0.59\, Wm^{-1}K^{-1}$, $C_{p_1} = 4.14 \times 10^3\, Jkg^{-1}K^{-1}$, $\beta_2 = 2.36 \times 10^{-4}\, K^{-1}$. *The parameter values for the fibres are shown in table 1.2*

	Rayon	**Nylon**	**Polyester**
R (m)	13×10^{-6}	30×10^{-6}	13×10^{-6}
$\tan\delta_2$	0.125	0.2	0.1
υ_2	0.3	0.4	0.4
$\rho_2(\mathrm{kgm^{-3}})$	1400	1140	1340
$c_2(\mathrm{ms^{-1}})$	1090	1340	5860
$K_2(\mathrm{Wm^{-1}K^{-1}})$	0.15	0.36	0.038
$C_{p_2}(\mathrm{Jkg^{-1}K^{-1}})$	1.5×10^3	1.42×10^3	1.02×10^3
$\beta_2(\mathrm{K^{-1}})$	36×10^{-5}	6×10^{-5}	1.7×10^{-5}

Table 1.2: Parameter values of the different fibres used in the numerical and analytical models

Note that in the insertion of asymptotic values for the Bessel and Hankel function as $r \to \infty$, Habeger's [1] expression appears to be missing a factor of 2. The attenuation is the sum to infinity of a series of B_{n_1} where n is an integer. However, when calculating the attenuation, the energy associated with the the higher order was assumed to be negligible and the series was truncated at $n = 2$. The attenuation calculated does not take into account the attenuation of the compressional wave through the water itself. This is, therefore, added to the attenuation of the fibres calculated above and is assumed to be $\alpha_1 = 25 \times 10^{-15} f^2$ taken from [6], where f is the frequency.

The effects of the additional assumptions that were made to derive the analytical model can be assessed by comparing the attenuation predicted by the analytical solution presented here and the numerical solution presented by [1]. These assumptions are that the acoustic attenuation from thermal processes are negligible and that the viscous wave generated in the fluid is also negligible. The results of the differences between the predicted attenuation are shown in figure 2 for three different types of polymer fibres:

Rayon, Nylon and Polyester. In general the discrepancy in the results is proportional to the attenuation. The two curves for each fibre have a similar shapes, with the exception of Polyester at low frequencies. This exception is not further examined here. The effect the assumptions have depends on the frequency range and radius used as well as the fluid properties and the thermal properties of the fibre. In the cases examined here, the discrepancies are not large, although the effect these errors have on the parameter estimation needs to be assessed when the model is used in solving the inverse problem.

We have, therefore, a simplified expression for α that can be used in solving the inverse problem. It is a function of the material properties of the saturated fibre and the suspending fluid, the radius of the fibre and fibre volume fraction. The next step is then to verify the model with experimentally obtained values of attenuation from suspension of fibre with known material properties and uniform radius.

3 Experimental

The experimental setup consists of a broadband transducer with a centre frequency of 10 MHz (V311), manufactured by Panametrics, Waltham, MA, USA. A pulser/receiver 5072PR from Panametrics was used to excite the transducer and amplify the received signal. The signal was then digitized using a CompuScope 14100 oscilloscope card, by Gage Applied Technologies Inc., Lachine, QC, Canada, with 14-bit resolution and a sampling rate of 100 MHz. All data was stored in a computer for off-line analysis. The resulting time-domain waveforms were calculated using the average of 100 sampled waveforms to reduce random noise. Before the averaging, the sampled waveforms are aligned to reduce timing jitter by using a method proposed by [7]. A digital thermometer F250, by Automatic Systems Laboratories LTD, England, monitored the temperature both in the suspension under test and in the room. The temperature was used to calculate the speed of sound in the water [8]. The fibre suspension was carefully poured into the measurement cell and then stirred until the majority of the air bubbles were removed. The measurement cell is described in detail in [9]. The attenuation of the sample was calculated according to [10].

The fibre suspension was made of Nylon fishing line, (STROFT$^{\text{TM}}$ GTM) with a nominal diameter of 60 μm,[1] chopped to a length of approximately 4 mm. The Nylon was a polyamide copolymer tempered to improve its tensile strength. The fibres were weighed and mixed with water to a concentration of 0.5% by weight. They were then left in water for 3 days to stabilise the temperature and to allow the fibres to become fully saturated. To prevent the fibres from settling during the test the suspension was stirred gently. A set of 30 runs were taken each with an average of 100 pulses.

[1] Permissbile diameter fluctuation $\pm 1\,\mu$m, Permissible norminal size deviation $+38\,\mu$m

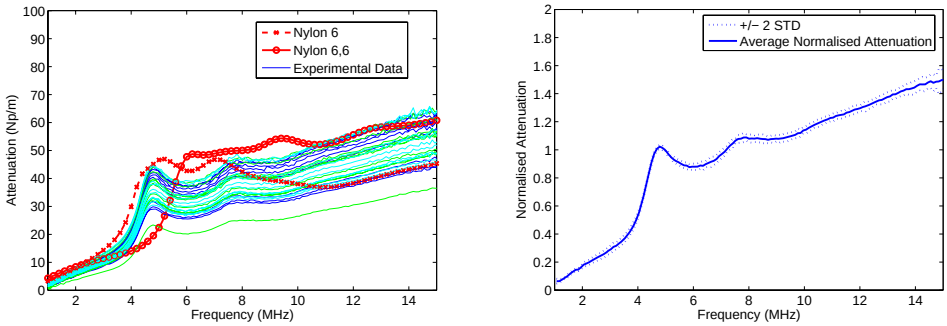

Figure 3: test

Figure 4: Attenuation as a function of frequency for a suspension of Nylon fibres in water at 0.5% concentration. Modelled and experimental attenuation values. Parameters for the saturated fibres are in shown in table 1.3. Right-hand figure is the Average of the Attenuation normalised by the value of the attenuation at 5MHz to remove the variance directly proportional to the attenuation.

4 Results

Figure 4 show the results from the 0.5% concentration of suspended Nylon fibres. As we can see there is a large variation in the level of attenuation although the shape of the curve is similar in all the measurement with local peaks in the attenuation at 4.8 MHz and at 7.7 MHz.

In the right-hand figure 4, the attenuation has been normalised by the value of the attenuation at 5MHz to remove the effect of variance directly proportional to the attenuation. Attenuation proportional variance is thought to be due to the inherent inhomogeneity of the suspension as the attenuation is proportional to the volume fraction. The fibres form flocs and through a combination of stirring and settling each time an ultrasonic pulse is emitted it travels through a different arrangement of fibres resulting in a different volume concentration and hence a different attenuation. The remaining variance, shown in the normalised attenuation graph increases with increasing attenuation and this is thought to be due to an decrease in the signal to noise ratio at the higher levels of attenuation found at higher frequencies.

The modelled attenuation is plotted in figure 4 with two possible set of parameters which are listed in table 1.3. The material properties are however, difficult to establish. The density was taken from the manufacturer data sheet, and adjusted for 5% water absorption. The speed of sound in Nylon 6 was taken from Habeger [1], whereas for Nylon 6,6 although the rod velocity was taken from his measurements in saturated fibres, Poisson's ratio in Nylon 6,6 was taken as 0.39 [11]. This means the speed of sound in Nylon 6,6 was calculated as 2345 ms^{-1}. Poisson's ratio for Nylon 6 was taken as the value that gave the best fit in Habeger[1] experiments. The exact value of the loss tangent was

	Nylon 6	**Nylon 6,6**
R (μm)	46.8 ± 0.4	46.8 ± 0.4
$c_2(\mathrm{ms}^{-1})$	1340	2345
$\rho_2(\mathrm{kgm}^{-3})$	1131	1131
υ_2	0.3	0.39
$\tan\delta_2$	0.2	0.15

Table 1.3: Parameter values used for Nylon

adjusted to best fit the experimental data as it can vary from very low, 0.01, in lightly crossed amorphous polymer to 3 depending on the molecular structure [12].

As the plots show, neither Nylon 6 or Nylon 6,6 fits the whole range. Nylon 6, gives a good fit for the low frequencies and Nylon 6,6 for the higher frequencies. The wide margin of error in the elastic constants and hence the speed of sound and the fact that the Nylon used was a polyamide copolymer, tempered to improve its tensile strength, could explain some of the discrepancies between the model results and the experimental results. Other explanations are that the values of the material parameters are not constant across the frequency range we are examining or that some of the fibres are not freely suspended but interact with one another which results in unpredictable ultrasonic attenuation. Multiple scattering would also cause differences between predicted and experimental results.

The peaks are thought to correspond to the resonant absorption at the eigenfrequencies of the cylinder, possibly of the shear wave, as opposed to reflections of internal waves from the ends of the fibres. This is because the peaks appear in both the experimental and the modelled values of attenuation and the modelled values are based on cylinders of infinite length.

5 Conclusions

In conclusion, we have established an analytical model relating the attenuation of ultrasound, in a suspension of fibres in a low viscosity fluid, to the material properties of the fibres. This model is amenable for use in solving the inverse problem of determining material properties of saturated fibres from measurements of attenuation. The results of the experiments indicate that the Nylon tested, a polyamide copolymer, has properties between that of Nylon 6 and Nylon 6,6. The material properties of saturated fibres are difficult to assess and hence have large margin of error. The results suggests that the model is sufficiently sensitive to material properties to detect differences in different types of Nylon.

The additional assumptions made that allow the analytical solution to be derived causes some discrepancies in the calculation of attenuation. However, the large variations in attenuation thought to be due to the inherent inhomogeneity, is likely to mask these differences.

6 Further Work

The elastic properties of the saturated Nylon fibres need to be investigated with an alternative method to verify that they do indeed lie between that of Nylon 6 and Nylon 6,6. Investigations at different concentrations need to be carried out to test if the inhomogeneity of the attenuation is the cause of the attenuation proportional variation.

Further work needs to be done to establish the cause of the local peaks in the frequency response of the attenuation. By testing other materials and different diameters of fibres the accuracy of the model can be assessed further.

The next step is then to use this model in solving the inverse problem in suspensions of greater complexity such as paper pulp where online data on the material properties of wood fibre in suspension is required. For this, a method for optimising the fitting of the modelled attenuation to the experimental values needs to be developed. The effects of non-uniform diameters and anisotropic nature of the pulp fibres also need to be assessed.

7 Appendix

Here, we have defined the elastic modulus involved in the vibratory motion as complex and equal to:

$$M_2(\omega) = M_2' - iM_2'', \quad \text{where} \quad M_2(\omega) = \lambda_2(\omega) + 2\mu_2(\omega) \tag{24}$$

$\tan\delta_2$ is then defined as the phase difference between the real and imaginary part of the elastic modulus:

$$\tan\delta_2 \quad = \quad -\frac{M_2''}{M_2'} \tag{25}$$

Denoting the compressional speed of sound in the solid as complex where $\mathbf{c_2} = c_2' - ic_2''$ we get

$$c_2'^2 - c_2''^2 = \frac{M_2'}{\rho_2}, \qquad 2c_2'c_2'' = \frac{M_2'\tan\delta_2}{\rho_2} \tag{26}$$

As $\tan\delta_2$ is small at the limit $\tan\delta \to 0$, which is the equivalent of assuming $c_2' \gg c_2''$ we get,

$$\mathbf{c_2} \quad \approx \quad c_2'\left(1 - i\frac{\tan\delta_2}{2}\right) \tag{27}$$

With the additional assumption that $k_{c_2}' \gg k_{c_2}''$ we get the same expression as derived by [13]. For ease of readability in the main text, the prime that distinguishes the real from the imaginary part has been dropped. So, in the main text, $c_2 = c_2'$.

μ_2 can be expression in terms of Poisson's ratio, υ_2 and the complex speed of sound using (24) and (27), if we assume that Poisson's ratio is real at these frequencies.

$$\mu_2 \quad = \quad \left(\frac{0.5 - \upsilon_2}{1 - \upsilon_2}\right) c'^2\rho_2(1 - i\tan\delta_2) \tag{28}$$

References

[1] C. Habeger, "The attenuation of ultrsound in dilute polymeric fiber suspensions," *Journal of Acoustical Society of America*, vol. 72, pp. 870–878, sep 1982.

[2] P. Epstein and R. Carhart, "The absorption of sound in syspensions and emulsions. i. water fog in air," *The Journal of the Acoustical Society of America*, vol. 25, pp. 553–565, May 1953.

[3] J. Allegra and S. Hawley, "Attenation of sound in suspension and emulsions: Theory and experiments," *The Journal of the Acoustical Society of America*, vol. 51, pp. 1545–1564, 2 1972.

[4] M. Morse, P and K. Ingard, *Theoretical Acoustics*, ch. 8, p. 13. Princetown University Press, 1986.

[5] P. Morse and H. Feshbach, *Method of Theoretical Physics*, vol. II, ch. 13. McGraw-Hill Book Company, Inc, 1953.

[6] L. Kinsler, A. Frey, A. Coppens, and J. Sanders, *Fundamentals of Acoustics*, ch. 8. Wiley, 4 ed., 1999.

[7] A. Grennberg and M. Sandell, "Estimation of subsample time delay differences in narrowband ultrasonic echoes using the hilbert transform correlation," *IEEE Transactions on Ultrasonics, Ferroelectrics, and Frequency Control*, vol. 41, no. 5, pp. 588–595, 1994.

[8] N. Bilaniuk and G. S. K. Wong, "Speed of sound in pure water as a function of temperature," *The Journal of the Acoustical Society of America*, vol. 93, no. 4, pp. 2306–2306, 1993.

[9] T. Löfqvist, "Ultrasonic wave attenuation and phase velocity in a paper-fibre suspension," in *Proc.IEEE Ultrasonics Symposium*, vol. 1, pp. 841–844, Oct 1997.

[10] D. McClements and P. Fairley, "Frequency scanning ultrasonic pulse echo reflectometer," *Ultrasonics*, vol. 30, pp. 403–405, 1992.

[11] L. Pedersen, "Tables of acoustic properties of materials," 2002.

[12] J. Ferry, *Viscoelastic Properties of Polymers*, ch. 2, pp. 46–47. John Wiley & Sons Inc, 3rd ed., 1980.

[13] M. Povey, *Ultrasonic Techniques for Fluid Characterization*, ch. A.4, p. 179. Academic Press, 1997.

Paper B

Ultrasonic Measurements and Modelling of Attenuation and Phase Velocity in Pulp Suspensions

Authors:
Jan Niemi, Yvonne Aitomäki and Torbjörn Löfqvist

Reformatted version of paper originally published in:
Proceedings of IEEE Ultrasonic Symposium, pp.775-779 (Rotterdam, Holland),2005

Ultrasonic Measurements and Modelling of Attenuation and Phase Velocity in Pulp Suspensions

Jan Niemi, Yvonne Aitomäki and Torbjörn Löfqvist

Abstract

In the manufacturing process of paper the mass fraction and material properties of the fibres in the pulp suspension are important for the quality of the finished product. This study presents two different methods of pulp characterisation. The first is based on phase velocity, which we use to investigate the composition of the pulp. Here a method is presented where the optimal number of circular shifts within the sampling window of the signal is determined which gives, in a weakly dispersive medium, a continuous phase spectrum and minimizes the likelihood of discontinuities within the bandwidth. Hence, the ambiguity in phase unwrapping is avoided. The results from phase velocity measurements show that the phase velocity weakly increases with increasing amount of fines in the suspension. The dispersion is caused by the fibres and it correlates with fibre mass fraction. The second method is based on attenuation and is used to characterise the wood fibres. The results of the attenuation experiments show that it is possible to inversely calculate wood fibre properties by fitting the model to the experimental data, if the fibre diameter distribution is known. However, the accuracy of these calculation is difficult to determined and more work in this area is required.

1 Introduction

In the manufacturing process of paper the mass fraction and material properties of the fibres in the pulp suspension are important for the quality of the finished product. When using recycled paper, fibres with unknown and varying material properties enter the process. Therefore, there is an increasing demand for methods of on-line characterisation of the pulp suspension as well as the fibres in suspension.

This study presents two different methods of pulp characterisation. The first is based on phase velocity, which we use to investigate the composition of the pulp. The second is based on attenuation and is used to characterise the wood fibres.

In the first method, we investigate how the phase velocity changes with different mass fractions of fibres and fines. To determine the phase velocity, a method is proposed based on a method by [1], where the an echo is circularly shifted an optimal number of samples.

In the second method, to be able to characterise the wood fibres, we use an analytical model which relates the material properties of saturated fibres to the attenuation. We then aim to solve the inverse problem of identifying which values result in the best fit of the model to the attenuation values calculated from experiments.

2 Phase Velocity

2.1 Theory and experiments

When determining the phase velocity from pulse-echo measurements, one encounters the problem of performing a correct phase unwrapping. The problem is well known and has been addressed in earlier investigations, for instance [2]. The problem arises when the phase velocity is calculated from the phase spectra of a the Fourier transform of each of the two echoes. In this study, we propose a method, termed Minimum Phase Angle (MPA), that determines an optimal number of circular shifts to the windowed signal which results in a continuous phase spectrum and minimizes the likelihood of discontinuities within the bandwidth. Therefore the ambiguity in the phase unwrapping is avoided. To experimentally test the method experiments were performed in pulp fibre suspensions, which are weakly dispersive. The experiments were carried out using the pulse-echo technique in a custom designed test cell. A schematical view of the measurement cell used in this study is shown in Fig. 1.

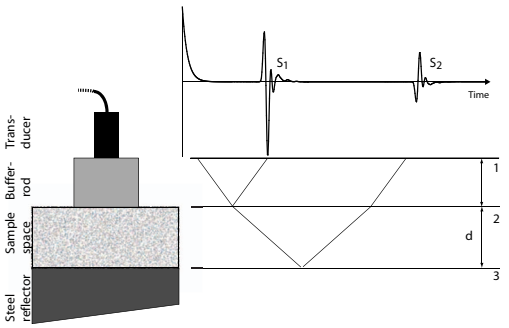

Figure 1: Lattice diagram of the pulse-echo measurement system used this study

The echoes from the interfaces depend on the initial pulse pressure amplitude $p_0(t)$ emitted from the transducer and the reflection and transmission coefficients of the different interfaces. For simplicity, we omit the reflection and transmission coefficients and the attenuation. With these assumptions, the echoes from the interfaces between the buffer rod/suspension and suspension/steel reflector are

$$P_1(\omega) = P_0(\omega)e^{-2j\frac{\omega}{c_1}d_1} = P_0(\omega)e^{-j\varphi_1(\omega)} \quad (1)$$

$$P_2(\omega) = P_0(\omega)e^{-2j\omega(\frac{d_1}{c_1}+\frac{d_2}{c_2})} = P_0(\omega)e^{-j\varphi_2(\omega)} \quad (2)$$

where $P_1(\omega)$ and $P_2(\omega)$ are the Fourier transform of the echoes $p_1(t)$ and $p_2(t)$, respectively. d_1 and d_2 are the distance in respective medium. The factor 2 above comes

from that the fact the pulse is travelling back and forth through the medium. c_1 and c_2 are the velocities in the buffer rod and pulp suspension, respectively. $P_0(\omega)$ is the Fourier transform of the initial emitted pulse from the transducer. Note that echo $p_1(t)$ has an extra phase shift of π compared to $p_2(t)$.

2.2 The method of minimum phase angle

To reduce the ambiguity in the phase unwrapping the following method is proposed.

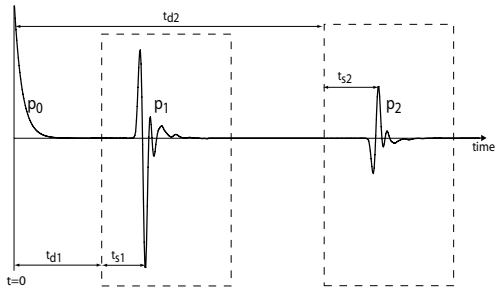

Figure 2: The received signal with illustrations of the time delays and time shifts

The sampled signal is divided into two sampling windows with time delays $t_d = n_d/f_s$ shown in Fig. 2 where n_d is the number of samples that the sampling window is delayed and f_s is the sampling frequency. Within each sampling window the signal is circularly shifted sample by sample. At each shift, a calculation of the phase angle is carried out as

$$PA = \frac{1}{f_2 - f_1} \sum_{m=f_1}^{f_2} \varphi_m^2 \tag{3}$$

where φ_m is the phase spectrum within the frequency bandwidth of $f_1 < m < f_2$ of the shifted sample. Thereafter a sign shift of the echo is carried out, representing a phase shift of π, and again circularly shifted and calculated with the same method. The results are compared and the circularly shifted sample that gives a phase spectrum without discontinuities and minimum value of PA is then chosen. The outcome is then the optimal time shift of $t_s = n_s/f_s$ where n_s is the number of samples the signal is shifted.

This results in two time delays, the time delay from the sampling window and time delay from the circular shift within the window. This gives the phase spectrum for the

respective echoes as

$$\varphi_1(\omega) = \phi_1(\omega) + \omega(t_{d1} + t_{s1}) \quad (4)$$

$$\varphi_2(\omega) = \phi_2(\omega) + \omega(t_{d2} + t_{s2}) \quad (5)$$

where ϕ_1 and ϕ_2 are the respective phase spectra of the circularly shifted signal. t_{d1} and t_{d2} are the time delay for respective sampling window. t_{s1} and t_{s2} are the circular shift within respective sampling window. An illustration of how PA changes when echo $p_1(t)$ is circularly shifted within the sampling window is shown in Fig. 3. In this example, the minimum of PA is found when $p_1(t)$ is shifted 100 samples to the left and inverted. Fig.2.3(c) shows the phase spectrum at the minimum of PA for $p_1(t)$ and $-p_1(t)$. We can see that the inverted signal has a phase spectrum with the minimum likelihood of a discontinuity being present in the spectrum.

The phase velocity for a pulp suspension sample can be expressed using (1)-(2) and (4)-(5) as

$$c_2(\omega) = \frac{\omega 2d_2}{\omega(t_2 - t_1) + \theta(\omega) - \theta_d(\omega) + m\pi} \quad (6)$$

where $t_1 = t_{d1} + t_{s1}$, $t_2 = t_{d2} + t_{s2}$, $\theta(\omega) = \phi_2(\omega) - \phi_1(\omega)$, $\theta_d(\omega)$ is the phase difference due to diffraction [3] and m is a correction term if a phase shift of π is added by the proposed method. In this study $m = 0$ if the proposed method inverts $p_1(t)$ to compensate for the extra phase shift that occurred, $m = 1$ if $p_1(t)$ and $p_2(t)$ are not inverted and $m = -1$ if both $p_1(t)$ and $p_2(t)$ are inverted.

2.3 Experiment

The experimental setup consists of a broadband transducer with a centre frequency of 10 MHz (V311), manufactured by Panametrics, Waltham, MA, USA. A pulser/receiver 5072PR from Panametrics was used to excite the transducer and amplify the received signal. The signal was then digitized using a CompuScope 14100 oscilloscope card, by Gage Applied Technologies Inc., Lachine, QC Canada, with 14-bit resolution and a sampling rate of 100 MHz. All data was stored in a computer for off-line analysis. The resulting time-domain waveforms were calculated off-line using the average of 100 sampled waveforms to reduce random noise. Before the averaging process, the sampled waveforms are aligned to reduce timing jitter by employing a method proposed by [4]. A digital thermometer F250, by Automatic Systems Laboratories LTD, England, monitored the temperature both in the suspension under test and in the room. The temperature in the pulp suspensions under test was $20.0 \pm 0.2°C$. The pulp suspensions was carefully poured into the measurement cell and thereafter stirred slowly to remove air bubbles from the suspension. An illustration of the measurement cell is shown in Fig. 1 and is described in detail in [5]. To accurately determine the distance d_2 in the cell, pure, distilled water was used as a reference since it has a well known relationship between speed of sound and temperature, see [6]. Using the temperature of the calibration fluid

and a cross-correlation technique to determine the time-of-flight for an ultrasonic pulse, the distance d_2 was found to be 0.03010± 0.00004 m.

The pulp samples used in this study were produced from thermo-mechanical pulp (TMP). The TMP was fractionated by Bauer-McNett fractionator according to SCAN-standard 6:69 [7]. This process separated the pulp into two fractions; a fibre fraction and a fines fraction. The fibre fraction consists of fibres that passed the 48 wire mesh, resulting in fibre lengths that vary between 1-3 mm and diameter of 20-50 μm. The fines were obtained by passing the pulp through the 200 wire mesh and then subsequently filtered through 400 wire mesh. They have a length of 30-74 μm and a diameter of a few μm. Both the fines and fibre size distributions were analyzed using a Kajaani Fiberlab instrument, Metso Corporation, Finland. From these fractions, a set of samples were made by mixing fibres and fines at predetermined ratios between 0-1.0% by mass.

2.4 Results

The results from the phase velocity measurement for suspensions containing only fines is shown in Fig.4. The figure shows that the velocity dispersion is small within the bandwidth of the ultrasonic pulse, 1.8-10 MHz, and that the phase velocity increases with increasing amount of fines in the suspension.The uncertainty in the measurement is ±0.3 m/s based on ±2 standard deviations.

Fig. 5, shows measurements of phase velocity for samples where the mass faction of fibres are the same as for fines. In this case, the velocity dispersion is noticeable and it is seen to correlate well with mass fraction, giving higher velocity dispersion with higher mass fraction. As an example, the velocity for 1.0% mass fraction changes from the lowest below 4 MHz to be the highest above.

3 Attenuation

3.1 Theory

The model is based on calculating the energy loss in the scatter wave from an infinitely long, viscoelastic, isotropic, cylindrical fibre. It is described in full in [8]. In [8], the modelled attenuation agrees well with experimental results of synthetic fibres such as nylon and shows localised extrema in the frequency response of attenuation. These peaks in frequency response of the attenuation are thought to be at the vibrational modes of the fibres. Although the locations of these peaks depend largely on the diameter of the saturated fibres, they also depend on their material properties.

In nylon, the locations of the peaks are more repeatable and hence more reliable than the measurement of the attenuation itself which varies due to the inhomogeneous nature of the suspension. The repeatability of the frequency at which these peaks occur and the fact that changes in diameter, Poisson's Ratio, Young's Modulus and the density of the fibre produce different effects on the shape of the modelled frequency response of the

attenuation, means that the suspension can be better characterised if these extrema can be located.

The aim is, therefore, to determine if localised extrema also exist in the frequency response of the attenuation of wood fibres. This would allow us to solve the inverse problem with less ambiguity than attempting to solve the inverse problem from a simple curve.

The model shows the attenuation in the frequency range 1Mhz to 25MHz to be very sensitive to fibre diameter. Using an average fibre diameter of 40 μm localised maxima in attenuation were predicted to be between 5MHz to 10MHz. However, the wood fibres in paper pulp have different diameters hence the diameter distribution of the wood samples is required to produce expected attenuation.

3.2 Experiment

The same measurement cell and paper pulp samples were used as in the phase velocity experiments. As the diameter of wood fibres are smaller than nylon the peaks are expected to appear at a higher frequency. Hence a 30MHz transducer (Panametric V333) was used and the signal digitised by a CompuScope 102G oscilloscope card (Gage Applied Technologies, Inc Lachine QC Canada) with a 10-bit resolution and a sample rate of 2GHz. The distance the signal travelled was calculated using the method previously described. Since the initial echo from the buffer rod could not be easily identified, the attenuation in the sample was obtained using pure, distilled water as reference giving,

$$\alpha_s(f) = \alpha_w(f) + \frac{1}{2d_2} ln \left(\frac{|P_w(f)|}{|P_s(f)|} \right) \quad (7)$$

where α_s is the attenuation in the sample, d_2 is the distance travelled by the signal, $P_s(f)$ is the amplitude in the frequency domain of the second echo in the sample and $P_w(f)$ is the amplitude in the frequency domain of the second echo in water. $\alpha_w(f)$ is the attenuation of water [9] and is assumed to be

$$\alpha_w(f) = 25 \cdot 10^{-15} f^2 \quad (8)$$

3.3 Results

Figure 6 is a comparison of the experimentally calculated average attenuation and the modelled attenuation. Good agreement has been obtained by adjusting the saturated wood fibre properties. The maximum at 2.2MHz in the experimental results is not reflected in the model results though a small maximum does exists at 2.4MHz and a slightly large one at 3.2MHz, corresponding to fibres with diameters of 60 μm and 40μm respectively. This lack of agreement could be because the model is for a fibre that is continuous over its cross section. As wood fibres are hollow the vibrational modes, which are believed to be causing the maxima, will not occur at the frequencies predicted by the model. However, it may also be due differences between the distribution of the diameters in this particular sample and that used in the size analysis. The peak could also be an

experimental artifact. The sensitivity of the modelled attenuation on the fibre diameter, means the distribution of the diameters is the dominant factor in determining the material properties of the suspended fibres. With unknown fibre diameter distributions, there is a greater possibility of determining the diameters of the fibres if the local extrema in the frequency response of the attenuation are clear. However, the superposition of maxima and minima of one wood fibre diameter with other fibres of a different diameters results in a the smoothing of the signal, masking the effects of the individual fibres. The featurelessness of the curve means that the calculation of the material properties from the experimental measured attenuation is ambiguous. Combinations of different values can give similar results.

4 Conclusion

In this study we have considered measurements of phase velocity and attenuation in pulp suspensions. The proposed method to calculate phase velocity avoids the ambiguity with phase unwrapping if the medium is weakly dispersive. The result shows that the phase velocity increases with increasing amount of fines in the suspension. The dispersion is caused by the fibres and it correlates with fibre mass fraction.

The results of the attenuation experiments show that it is possible to inversely calculate wood fibre properties by fitting the model to the experimental data, if the fibre diameter distribution is known. However, the accuracy of these calculation is difficult to determined and more work in this area is required.

5 Further Work

The proposed minimum phase angle, or MPA, method has to be tested in cases when the phase velocity is highly dispersive.

The peak in the experimental results of the frequency response of attenuation at 2.2MHz needs further investigation. Experiments on synthetic fibres are being carried out to explore the effect of hollow compared to solid fibres. If these effects are significant, further development of the model is required to take this into account.

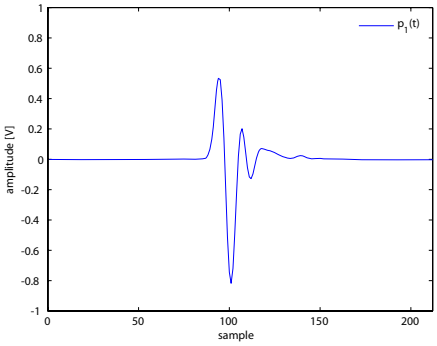

(a)

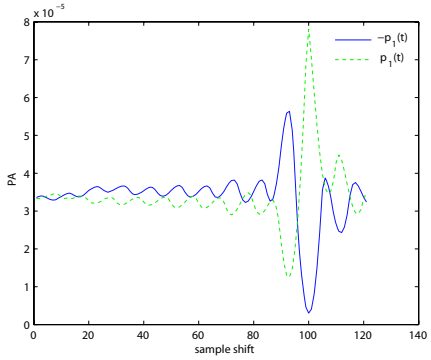

(b)

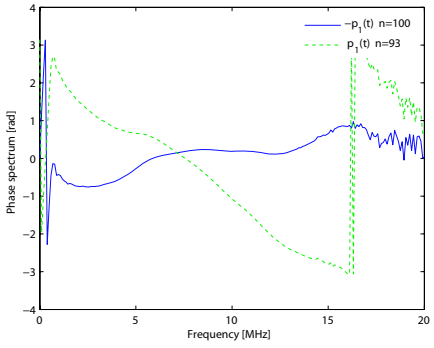

(c)

Figure 3: (a) shows echo $p_1(t)$. (b) shows the results of $pa(m)$ from $p_1(t)$ and when $p_1(t)$ is inverted. (c) shows the phase spectrum of $p_1(t)$ and $-p_1(t)$ when the echoes are shifted 93 and 100 samples respectively, i.e at respective minimum of pa

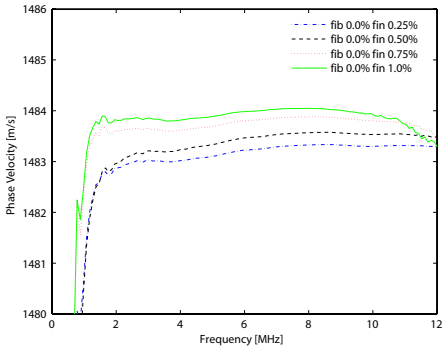

Figure 4: Phase velocity in pulp suspension containing fines and no fibres

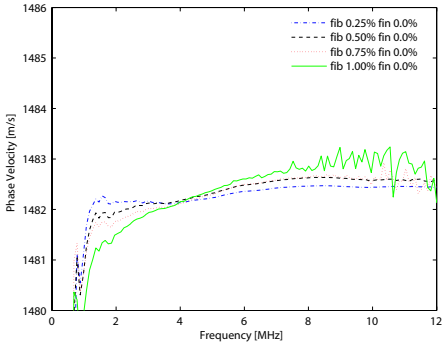

Figure 5: Phase velocity in pulp suspension containing fibres and no fines

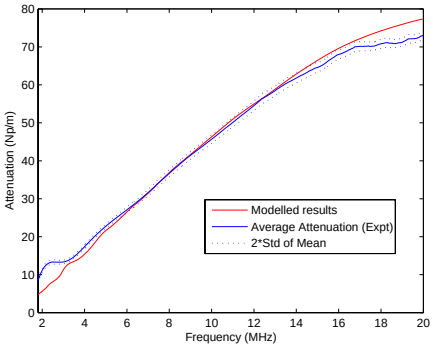

Figure 6: Comparison of the modelled attenuation to the measured attenuation for 0.5% concentration of wood fibres. Plot of the mean and 2x STD of the mean for 300 readings. The following material properties for saturated wood fibres were used in the model: density=1500 kg/m^3, Poisson ratio = 0.45, speed of sound= 1050 m/s and loss tangent=0.2. The properties of water were assumed to be: density=996 kg/m^3, speed of sound=1490 m/s, and viscosity=$9.4 \cdot 10^{-4} Pa \cdot s$

References

[1] P. He, "Experimental verification of models for determining dispersion from attenuation," *IEEE Transactions on Ultrasonics, Ferroelectrics, and Frequency Control*, vol. 46, no. 3, pp. 706–714, 1999.

[2] J. Tribolet, "A new phase unwrapping algorithm," *IEEE Transactions on Acoustics, Speech, and Signal Processing*, vol. 25, no. 2, pp. 170–177, 1977.

[3] P. Rogers and A. Van Buren, "An exact expression for the lommel diffraction correction integral," *Journal of the Acoustical Society of America*, vol. 55, no. 4, pp. 724 – 8, 1974.

[4] A. Grennberg and M. Sandell, "Estimation of subsample time delay differences in narrowband ultrasonic echoes using the hilbert transform correlation," *IEEE Transactions on Ultrasonics, Ferroelectrics, and Frequency Control*, vol. 41, no. 5, pp. 588–595, 1994.

[5] T. Löfqvist, "Ultrasonic wave attenuation and phase velocity in a paper-fibre suspension," in *Proc.IEEE Ultrasonics Symposium*, vol. 1, pp. 841–844, Oct 1997.

[6] N. Bilaniuk and G. S. K. Wong, "Speed of sound in pure water as a function of temperature," *The Journal of the Acoustical Society of America*, vol. 93, no. 4, pp. 2306–2306, 1993.

[7] Scandinavian Pulp, Paper and Board Testing Committee, Stockholm, *SCAN-M 6:69, Fibre fractionation of mechnical pulp in the McNett apparatus.*

[8] Y. Aitomäki and T. Löfqvist, "Measuring suspended fibre material properties by modelling ultrasound attenuation," in *Mathematical Modelling of Wave Phenomena*, 2005. To be published.

[9] L. Kinsler, A. Frey, A. Coppens, and J. Sanders, *Fundamentals of Acoustics.* John Wiley and Sons Inc., 4 ed. ed., 2000.

Paper C

Inverse Estimation of Material Properties from Ultrasound Attenuation in Fibre Suspensions

Authors:
Yvonne Aitomäki and Torbjörn Löfqvist

Reformatted version of paper originally published in:
To be submitted to: Elsevier Ultrasonics.

Inverse Estimation of Material Properties from Ultrasound Attenuation in Fibre Suspensions

Yvonne Aitomäki and Torbjörn Löfqvist

Abstract

A model based on ultrasound scattering is experimentally verified for a dilute suspension of synthetic fibres in water. We then compare the accuracy of material properties of the fibres estimated from fitting the model to experimental measurements of attenuation to material properties of the fibres from other sources. The experimental results support the theory that the resonance peaks in the frequency response of the attenuation are a function of the diameter of the fibre. The estimated value of shear modulus is in line with previously reported values and the density is estimated to between 10% and 15%. Poisson's ratio is overestimated, leading to underestimation of the Young's modulus. This overestimation of Poisson's ratio is thought to be due to a lack of accuracy of the model at high frequencies. It appears that the accuracy of the estimation procedure depends on frequency range containing resonance peaks. Further work on the model is required to increase its accuracy at higher frequencies to improve the estimation of Poisson's ratio and Young's modulus.

1 Introduction

This study is part of ongoing research in the paper pulp characterisation using ultrasound. The quality of paper pulp depends on the large number of factors and some of these are the properties of the pulp fibre itself [1]. Monitoring pulp characteristics has, therefore, the potential to provide paper manufacturers with increased control over their pulp production. The measurement method being investigated is based on ultrasound, as it is rapid, inexpensive, non-destructive and non-intrusive. Consequently, such a measurements could be done online.

Two approaches that can be used to model ultrasound propagation in paper pulp are to model it either as a solid porous media or to as cylindrical scatters suspended in a fluid. The solid porous media approach has been applied to paper pulp using Biot's model of the attenuation and velocity of ultrasound [2]. However, the structural and solid/fluid interaction parameters are many and difficult to establish. Using dilute solutions and higher frequencies than the Biot model, scattering models can be considered. Epstein-Carhart [3]/Allegra-Hawley [4], (ECAH), model and the Harker and Temple model [5] have been developed for spherical like particles in suspension. A review of these theories concerning their use in determine particle size distribution is found in [6]. Most of the work has, however, been concentrated on spherical particles. Studies of cylindrical

particles have concentrated on large scatterers, where the product of the wave number and the radius, kR, is large. In these studies, back-scattering rather than attenuation is considered [7], [8].

One of the closest models to that of a suspension of pulp fibres in water is that developed by Habeger [9]. This is a cylindrical extension of the ECAH model and relates the attenuation to the properties of water, the properties of the fibre, and the fibre concentration. In the calculation of attenuation, the equations are based on a number of different material properties and are solved numerically. By neglecting thermal effects and assuming low viscosity in the suspending fluid, a more tractable set of equations is reached that can be solved analytically [10].

In this paper, we investigate whether this simplified cylinder scattering model (SCS) can be used to solve the inverse problem of estimating material properties of cylindrical particles in suspension from the attenuation of ultrasound across a range of frequencies. The aim is to apply this to pulp fibres suspended in water but since natural fibres have non-uniform diameters and have variable material properties, nylon fibres in water were used to test the accuracy of the estimation of material properties from experimentally obtained ultrasound attenuation.

We start by describing the simplified SCS model and the experimental procedure used to obtain the frequency response of attenuation of a suspension of nylon fibres in water. We discuss the results and ways in which they can be improved both by refining the theoretical model and the experimental procedure.

2 Theory

In the SCS model, the attenuation is calculated from the energy losses arising when a plane wave is incident upon an infinitely long, straight cylinder. The cylinder material is assumed to be isotropic and viscoelastic. The energy losses taken into account are from the wave being partially reflected, partially transmitted at the solid-fluid interface and from the generation of damped, transverse waves in the solid medium at the boundary. The highly damped thermal skin layer, that is generated by the acoustically induced pulsations of the solid is shown by [9] to have the greatest effect where the thermal wavelength is of the order of the radius. We therefore consider frequencies above this region, thus reducing the number of material properties in the solution and increasing the feasibility of estimating the remaining material properties from attenuation measurements. A viscous wave in the fluid (as defined by [3]) is also generated but due to the low viscosity, the energy loss due to this wave is small and is neglected. The derivation is presented by [10] and the resulting equation for the attenuation α is

$$\alpha = \frac{-2f_r}{\pi R^2 k_{c_1}} \sum_{n=0}^{\infty} \Re \left(\int_0^{\frac{\pi}{2}} \epsilon_n B_n \cos(\psi) d\psi \right) \tag{1}$$

where f_r is the volume fraction; R is the radius of the fibre; k_{c_1} is the wave number of the compressional wave in water; ψ is the angle of between the plane of the fibre and

the direction of the oncoming ultrasound wave; n is a positive real integer; ϵ_n has the value 1 if $n = 0$ otherwise $\epsilon_n = 2$ and where B_n is the n^{th} expansion coefficient of the wave potential of the reflected wave. With the assumptions stated above, the solution for the coefficients B_n, comes from using the boundary condition of continuous velocity in the radial direction and continuous stress in radial, tangential and axial directions at the fluid-solid interface. These conditions are expressed in terms of the wave potentials of the incident wave and reflected wave in the fluid and the compressional and shear wave potentials in the fibre. The result is an expression for B_n as a function of the fluid properties: viscosity, density and velocity of the compressional wave and the fibre properties: shear modulus, density, loss tangent, velocity of the compressional and shear waves. The shear modulus is a function of the density and velocity of the shear wave. The shear wave velocity is related to the compressional wave velocity by Poisson's ratio. The actual expression for B_n is solved using Maple© (Maplesoft, Waterloo, Canada). As can be seen in equation 2, the attenuation is a sum of B_n. In our experiments on nylon in water, four terms (n =3) were used, as higher terms did not have any significant effect on the attenuation in the frequency range we are considering. We note, however, from investigation of particulate solutions, it has been empirically established that the number of term to use is $n = 1.05k_{c1}R + 4$ [6].

We compensate for an assumption in the derivation of the attenuation that viscosity of water is neglected, once the expansion coefficients have be established, by adding the attenuation of water to the attenuation calculated by equation 2.

3 Experiment

The experiments were carried out using the pulse-echo technique. A schematic view of the measurement cell used in this study is shown in Fig. 1.

The attenuation of the sample can be calculated using distilled water as a calibration medium such that,

$$\alpha_E(f) = \frac{1}{2d} \ln(\frac{S_2'}{S_1}), \tag{2}$$

where f is the frequency, $S_1 = S_1(f)$ is the frequency dependant amplitudes of the first and $S_2' = S_2'(f)$ is the frequency dependant amplitudes of the calibrated second echo and d is the distance between the buffer rod and steel reflector. The calibration with water compensates for losses due to transmission at the sample-steel interface, transducer alignment and possible diffraction effects.

Three fibre suspensions were made up using different diameters of Nylon 66 fibres (Swissflock, Emmenbrücke, Switzerland). The fibres are identified by their fineness values and their dimension are given in Table 3. The fibres were weighed and mixed with distilled water to a concentration of 0.5% by weight.

The broadband transducer (V319, Panametrics, Waltham, MA, USA) used had a centre frequency of 15 MHz. The transducer was excited and the received signal amplified by a pulser/receiver (Model 5073PR, Panametrics). The signal was then digitized using

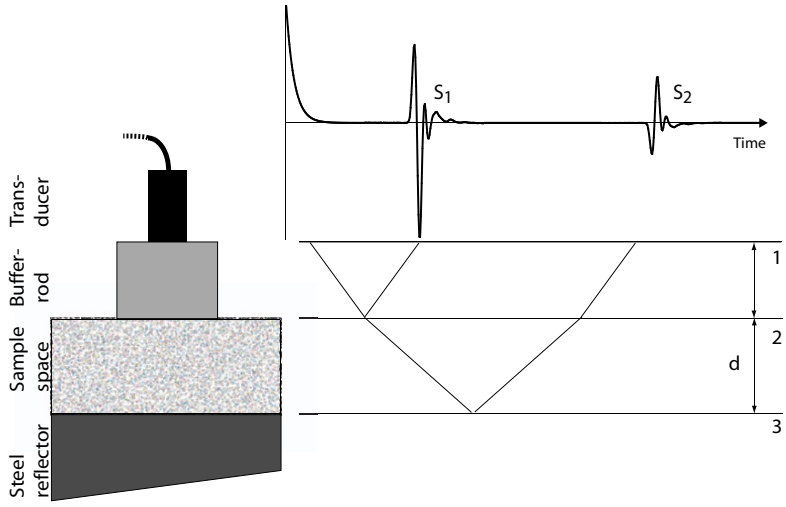

Figure 1: Lattice diagram of the pulse-echo measurement system used this study.

Fibre Fineness (dTex)	**Diameter ± 2xSTD (10^{-6} m)**	**Length (10^{-3} m)**
1.7	17.32 ±0.54	1.2
17	51.07 ±0.64	1.5
22	55.17 ±0.91	1.5

an oscilloscope card (CompuScope 12400, Gage Applied Technologies Inc., Lachine, QC, Canada) with a 12-bit resolution and a sampling rate of 400 MHz. All data were stored in a computer for off-line analysis.

Calculating the attenuation from each individual time-domain waveform and then averaging causes a bias in the results [11]. To reduce this bias the following procedure was used. The time-domain waveforms were aligned to reduce timing jitter using a method proposed by [12], then the discrete Fourier transform was applied to each echo. The frequency dependent amplitude of the second echo in the frequency domain, S_2', was then calibrated with the echoes from a sample of distilled water by letting

$$S_2' = S_2 \frac{A_2 K}{A_1}, \tag{3}$$

where S_2 frequency dependent amplitude of the second echo in the frequency domain, $A_1 = A_1(f)$ and $A_2 = A_2(f)$ are the frequency dependent amplitudes of the first and second echoes in water, K is the effect of the theoretical attenuation by water, $K = \exp(25 \cdot 10^{-15} f^2 2d)$ [13].

The echoes could then be averaged and the standard deviation calculated, using the technique described in [11]. Note that the noise in the signal from the distilled water

Material Property	Upper Value	Lower Value
Density (kgm^{-1})	900	2000
Wave velocity (compression wave) (ms^{-1})	500	7000
Poisson's ratio	0.2	0.5
Loss tangent	0	1

Table 3.1: Table of limits used in the parameter estimation procedure.

sample is assumed to be insignificant as the attenuation of the ultrasound in water is low, resulting in a high signal-to-noise ratio.

The cell was calibrated using water, emptied and carefully filled with the fibre suspension. Each measurement set consisted of a sequence of 100 pulses and their echoes. Five sets were taken and the sample was stirred after each reading. The cell was emptied and rinsed with temperature-controlled water, before the cell was filled with the next sample and the process repeated. Once all three samples were measured, the whole procedure was repeated twice more but with the samples measured in a different order.

A digital thermometer (Model F250, Automatic Systems Laboratories LTD, England) monitored the temperature in the sample under test. During the whole process the temperature of the suspension varied from a minimum of $20.75 \pm 0.2\,^{\circ}C$ to a maximum of $21.47 \pm 0.2\,^{\circ}C$. The temperature of the water during calibration was taken and used to calculate the wave velocity. The distance d of the measurement cell in Figure 1 was found using this wave velocity and a cross-correlation technique to determine the time-of-flight for an ultrasonic pulse.

Method for Parameter Optimisation

A non-linear least squares fit was found using a subspace trust region method and is based on the interior-reflective Newton method implemented by the *lsqnonlin* function in Matlab© (MathWorks, Inc., Natick, Massachusetts, USA). Since this function searches the whole number space, boundaries were implemented so that values outside reasonable limits were discarded. The limits are given in Table 3.1. Three initial values were used and are listed in Table 3.2. To optimise this procedure, the modelled attenuation calculation was simplified by assuming all the fibres were at a uniform angle of $\pi/6$ rather than integrating over the range 0 to $\pi/2$ for each iteration of the best-fit algorithm. The angle $\pi/6$ was used as this gave a close fit to the attenuation calculated when the whole range is used. Once the different initial starting points had either converged or timed out, the value to which they converged was used as the starting point for the slower, more accurate optimisation estimation where the attenuation is calculated from integrating over fibre angles from 0 to $\pi/2$.

Material Property	Set 1	Set 2	Set 3
Density (kgm^{-1})	1131	1000	1000
Wave velocity (compression wave) (ms^{-1})	1340	500	2500
Poisson's ratio	0.3	0.2	0.4
Loss tangent	0.2	1	0.1

Table 3.2: Table of Initial values used in the parameter estimation procedure.

4 Results and Discussion

4.1 Predicted and Experimental Attenuation

Figure 2 shows the predicted attenuation from the model using the material data from Table 6 in the Appendix and the diameters of the fibres used in the experiments. The peaks are believed to be caused by resonance in the fibres associated with the fibre diameter. The location in the frequency domain of these peaks is therefore a function of the diameter of the fibre, as seen in this figure where the material properties are kept constant and the fibre diameters change. The frequency range is chosen to match the bandwidth of the transducer. The results of the experimental attenuation calculations

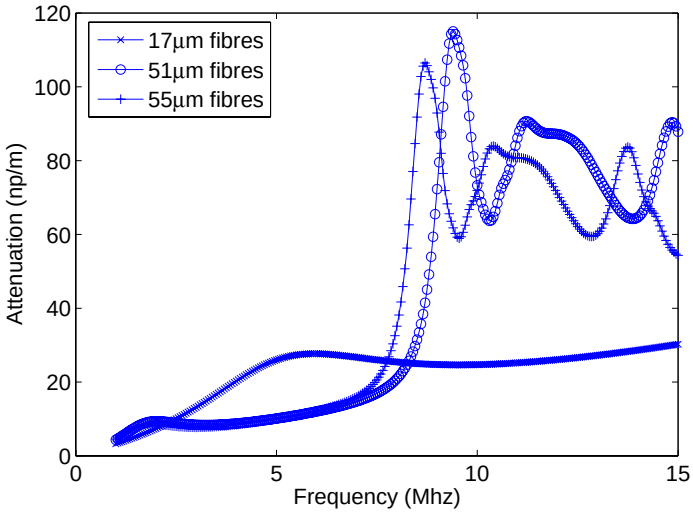

Figure 2: Predicted Attenuation for 17 µm, 51 µm and 55 µm Nylon 66 fibres using material data from Table 6.

for all three fibre diameters are shown in Figure (3). The standard deviations are small

in the chosen frequency region where the maximum standard deviation of the average is $0.6\,\mathrm{Npm}^{-1}$, $2.9\,\mathrm{Npm}^{-1}$ and $2.4\,\mathrm{Npm}^{-1}$ for the $17\,\mu$m, $51\,\mu$m and $55\,\mu$m fibres, respectively. The maximum standard deviation occurs at the higher frequencies where the signal-to-noise ratio is small.

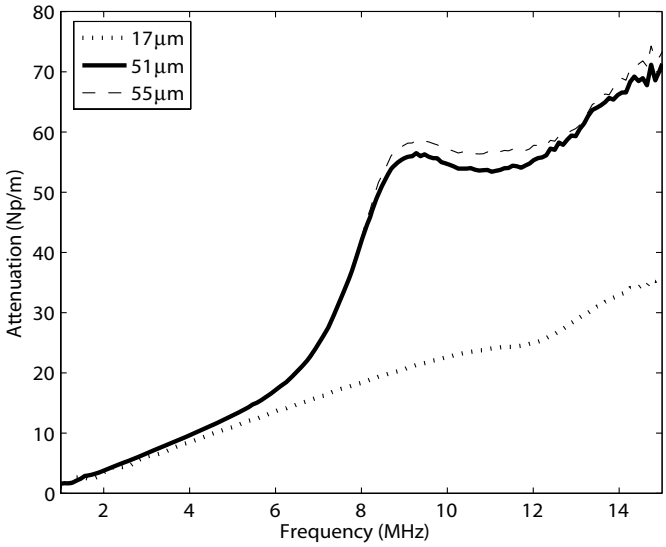

Figure 3: Experimental Attenuation for 17 μm, 51 μm and 55 μm Nylon 66 fibres.

The most notable aspect in comparing Figure 2 and Figure 3 is that either a damping mechanism is missing from the model or that the data available for the loss tangent is not accurate for these fibres. A plot of the tabulated data with the loss tangent set to 0.2 and the diameter set to $55\,\mu$m is shown in Figure 4 and shows that the predicted attenuation is now closer to the experimental attenuation. Although the fibres are different lengths, 1.2 mm compared to 1.5 mm, the appearance of a resonance peak for the $51\,\mu$m and the $55\,\mu$m fibre within 1 MHz of the predicted peaks supports the theory that the peaks in the attenuation are resonance peaks associated with the diameter of the fibres. The small difference in diameter between the $51\,\mu$m fibres and the $55\,\mu$m fibre does not result in a difference in the frequency of the peaks as predicted by the theoretical results. This is most likely caused by differences in the material properties of the fibres tested.

The problem of a lack of homogeneity of the fibre suspension is reduced by taking a large number of readings. On average the mass fraction of the measured suspension is

equal to that of the whole sample. The volume fraction is calculated as,

$$f_r = \frac{\rho_1 m_f}{\rho_2(1 - m_f)} \tag{4}$$

where m_f is the mass fraction, ρ_1 is the density of the water and ρ_2 is the density of the fibre. In the parameter estimation procedure, the mass fraction is kept constant. The volume fraction is therefore re-calculated with every iteration of the fit function for different values of density. Differences between predicted and observed attenuation

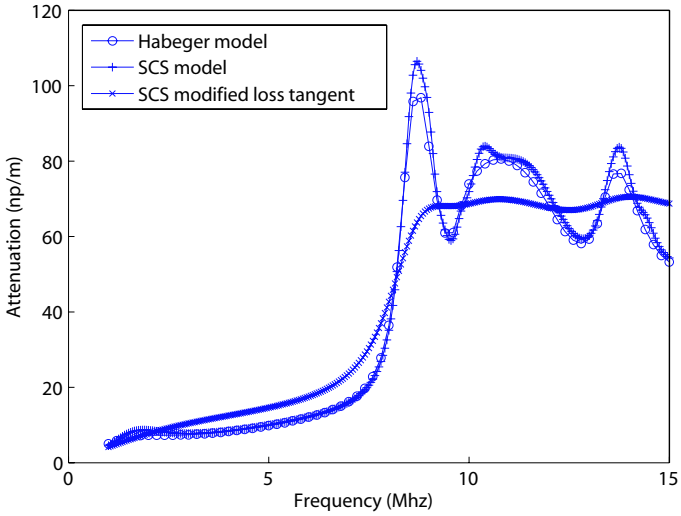

Figure 4: Predicted Attenuation from the complete numerical solution Habeger [9] and for the present model for 55 μm Nylon 66 fibres using material data from Table 6.

could also be due to neglecting both the thermal considerations and the generation of transverse waves in the water. Using the tabulated data, we can solve Habeger's equations numerical [9] to predict the attenuation to assess the error due to neglecting thermal and shear waves in the fluid. This is presented in Figure 4 and validates these assumptions, in this frequency range and for this fibre diameter and with these material properties.

Errors in the experimentally obtained attenuation exist from not adjusting the attenuation of water to the temperature of the suspension. The attenuation is assumed to be $25 \cdot 10^{-15} f^2$ Npm^{-1} throughout. Since the attenuation of water is used in the calibration, this may contribute to slight discrepancies at high frequencies.

4.2 Parameter Estimation

Figure 5 shows the theoretical attenuation using the estimated parameter values for each fibre diameter. As can be seen a close fit has been achieved for all three fibres diameters.

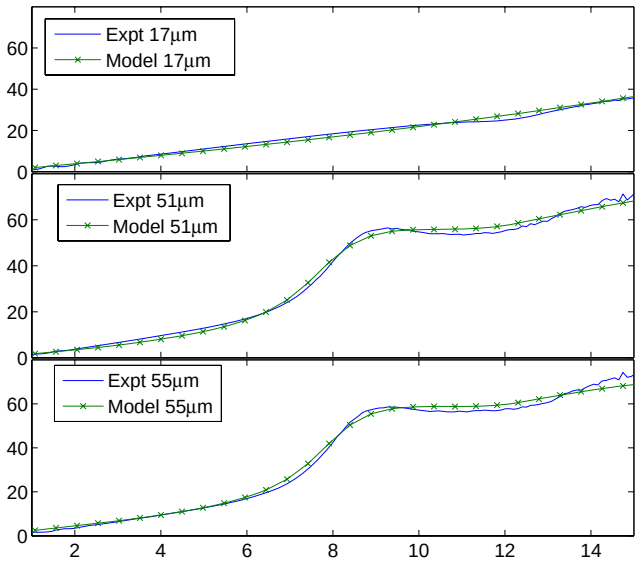

Figure 5: Plot of the experimental results and the best-fit lines for all the Nylon 66 fibres of different diameters.

The initial values found from the parameter estimation procedure for the 17 μm fibres overestimated the density by 50%. Since this is unrealistic, the results presented in Figure 6 for the 17 μm fibres are from the estimation procedure run with the density and loss tangent set to that of the 55 μm fibres so that comparisons of the estimated material properties can be made to known fibre properties.

However, this raises serious doubts on the possibility of using parameter estimation when data is only available in frequency range before the first resonance peak, such as is the case for the 17 μm diameter fibre. In this frequency range, with a fibre diameter of 17 μm, the number of combinations of values that that fit the monotonic curve seen in this region are too numerous or that the model is insensitive in this region to changes in the density and loss tangent. Evidence for the latter explanation comes from resonance scattering theory (RST) [8] where it is suggested that in between two eigenfrequencies the scatterer appears as an impenetrable object. Further work on the sensitivity of the

model in this region is required to establish this.

Estimations of the parameters were also calculated for the average attenuation ± 1 standard deviation. This gives us an indication of the sensitivity of the parameters to changes in attenuation. The density and Poisson ratio vary by max 0.8% and max 0.4%, respectively, whereas, the loss tangent and velocity have max variation of 3.1% and 6.8%. This variation consequently affects the Young's modulus and shear modulus, which have a max variation of 4.7% and 5.0% respectively.

A feature in the experimental curves that is not matched by either of the best-fit lines is the dip in the 17 μm fibre at 12 MHz (Figure 5). This could be caused by either experimental factors that has not been considered or by one of the model assumptions not being justified. This dip in attenuation coincides with dips in the attenuation of the 51 μm and 55 μm fibres, also at 12 MHz. The model assumes the cylinder is infinitely long but since the 17 μm and the larger diameter fibres have different lengths, this leads to conclude that the length is not causing the anomaly. It was however noted that the first echo in both water and the sample drops rapidly at this point so we concluded that experiments with different transducers are required to eliminate the possibility of this dip being an experimental artefact.

In manufacturing as the nylon is drawn into fibres, its molecules are aligned and its axial stiffness increases compared to bulk material [14], [15]. Values of axial Young's modulus are 5.7GPa [15]. However in [15] it is shown Young's modulus is 3.5 GPa in the transverse direction and found to be constant with draw ratio. Young's modulus, E, for the fibres is calculated from the density, ρ_2, Poisson's ratio, υ and the velocity of the compressional wave, c_2 as

$$E = \frac{(1+\upsilon)(1-2\upsilon)}{(1-\upsilon)}\rho_2 c_2^2. \tag{5}$$

The values for Young's modulus calculated from the estimated material values, presented in Figure 6, range from 2.05 GPa to 2.63 GPa. We would expect these values to be closer to the transverse values as it is assumed that as the angle of incidence of the sound wave to the fibre axis deviates away from the normal, more of the wave is reflected hence only a small proportion of the ultrasound wave propagates at an angle close to the fibre axis. Even considering that we should compare the results to the transverse value instead of the axial value, all these values appear to be underestimated by approximately 35%-50%.

The shear modulus, μ is calculated from

$$\mu = \frac{(0.5-\upsilon)}{(1-\upsilon)}\rho_2 c_2^2 \tag{6}$$

Using the estimated values for these properties, the shear modulus ranges from 0.68 GPa to 0.88 GPa (Figure 7). These findings are in good agreement with Wakelin *et al* [14] who gave values ranging from 0.62 GPa to 0.95 GPa. The agreement with [15] data is not as good, this may be because the difference in form of the nylon. In [15] film was tested and in [14] fibres were tested.

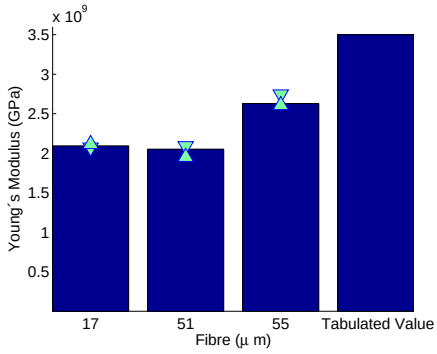

Figure 6: Chart of Young's modulus calculated from estimated material properties and the tabulated value of Young's modulus (Table 6).

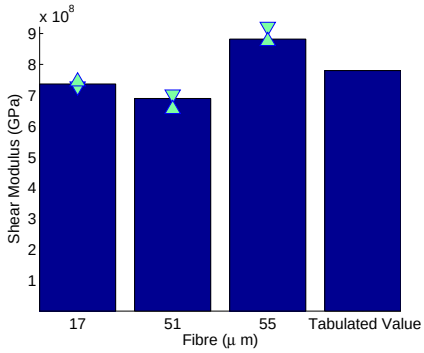

Figure 7: Chart of shear modulus calculated from estimated material properties and the tabulated value of shear modulus (Table 6).

The wave velocity (Figure 8) for the 17 μm fibre is estimated as 2030 ms^{-1}, which is comparable to 2345ms^{-1} [9] and 2620 ms^{-1} [16]. However, the values for the larger diameters appear to be overestimated. A possible explanation for this is that the model is not as accurate at high frequencies and tends to underestimate the attenuation possibly because additional attenuation processes exists that have not been taken into account. To compensate, the estimation process selects a value of c_2 much greater than the true value to reduce the error between the modelled and experimental attenuation values in this frequency region.

One possible reason for the lower prediction of attenuation at higher frequencies is the effect of neglecting multiple scattering. In the model the attenuation from a single particle is simply multiplied by the number of particles. These effects could potentially be approximated by adding the attenuation due to the loss tangent of the material, in proportion to the fibre fraction to the original calculation of attenuation in equation(2).

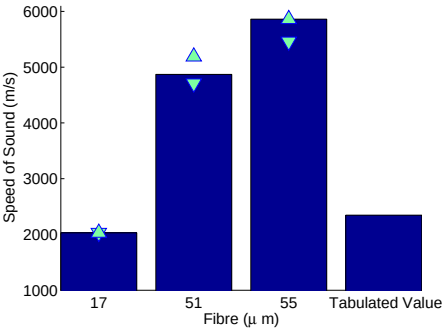

Figure 8: Estimated and tabulated values of velocity of the compression wave (Table 6).

Another reason for the lower prediction of the attenuation may come from modelling the fibre as an isotropic material. Adjustments to the model could be made for these effects, or the estimation process could be modified so that more weight is put on the match in the lower frequency region. These methods could potentially increase the accuracy of the estimation of the wave velocity.

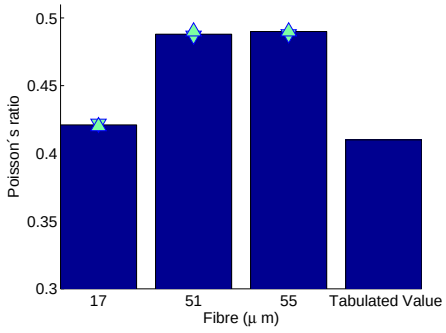

Figure 9: Estimated and tabulated values of Poisson's ratio (Table 6).

The estimated values for Poisson's ratio are 0.42 for the 17 μm fibres and 0.49 for the larger fibres. The 0.42 value is in agreement with other sources as indicated in Figure 9, however the 0.49 value is excessively high. The size of the shear wave speed, and hence the shear modulus, relative to the size of the compression wave speed, c_2 is set by Poisson's ratio. Hence, if the shear wave speed has been accurately estimated but the value of c_2 is overestimated, the result is an overestimation of Poisson's ratio. A consequence of overestimated values of Poisson's ratio is that Young's modulus will be

underestimated as can be seen from equation 5.

The estimates for density are shown in Figure 10 and show that it is overestimated in all three fibres. The density of bulk Nylon 66 is $1140\,\mathrm{kgm}^{-3}$ whereas the model overestimates density by 10% to 15%. The drawing of nylon has been shown to increase the density by 0.1% only [17] hence this cannot account for the difference in density seen here. The problem, highlight earlier, of the inaccuracy of the model at high frequencies causing Poisson ratio to be overestimated, could also cause the density to be overestimated.

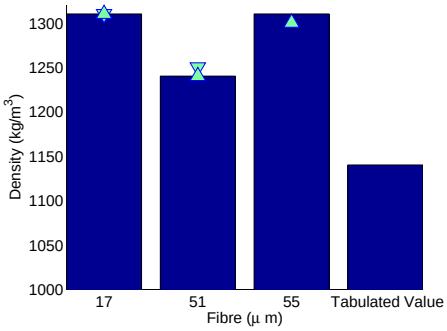

Figure 10: Estimated and tabulated values of density (Table 6).

The estimated loss tangent values are about 0.3, which is an order of magnitude larger than the values measured by [15] as shown in Figure 11. If we assume that the peaks in the attenuation are due to resonance, one possible explanation for this large discrepancy in the loss tangent is that it is being calculated from a point where the fibres are resonating (since the loss tangent for the $17\,\mu$m fibres was set to that of the $55\,\mu$m fibres). Hence, the amount of energy lost due to internal friction is probably higher at this point, where displacements are larger, than at other frequencies where the fibres are not resonating.

5 Conclusion

The experimental results support the theory that the resonance peaks are a function of the diameter of the fibre. Increasing the loss tangent of the material improves the fit considerably. This increase in value of the loss tangent may be more realistic under conditions of resonance.

The estimation process, in this study, is not reliable when only measurements from the frequency range before the first resonance peak is available, such as was the case for the $17\,\mu$m diameter fibre. This may be because the number of combinations of values that that fit the monotonic curve seen in this region is too great or that the model is

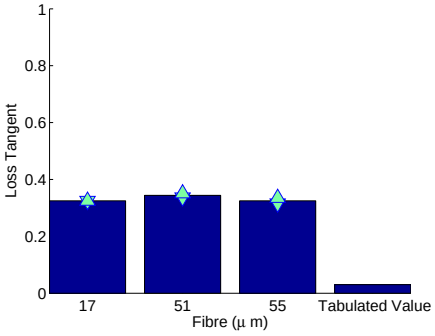

Figure 11: Estimated and tabulated values of Loss tangent (Table 6).

insensitive in this region to changes in the material properties of the fibre. Although further work is required, these findings suggest that in order to gain sufficiently accurate information on material properties of fibres, future studies should concentrate on the behaviour of ultrasound as it interacts with the fibre at a frequency as close as possible to the first resonance peak of the fibre.

The shear modulus values are in line with other sources. The density is overestimated by 10%-15%. However, the wave velocity, Poisson's ratio and consequently Young's modulus do not match values from other sources. Weighting the best-fit algorithm for lower frequencies or improving the accuracy of the model for high frequencies may reduce the overestimation of the wave velocity and Poisson's ratio and consequently decrease the value of Young's modulus.

Anisotropic effects may also cause the overestimation of the wave velocity and Poisson's ratio. The effect is difficult to predict and further work is required in this area.

The main issues that have to be addressed when applying this estimation method to paper pulp is the effect of non-uniformity of the fibre diameters, fibres curl and effects of the fibres being hollow.

6 Appendix

Material Property	**Value**	**Source**
Tensile modulus (axial, DR 3)	5.7 GPa	Leug *et al* [15]
Tensile modulus (transverse)	3.1 GPa	Leug *et al* [15]
Shear Modulus (fibre)	0.62 GPa -0.95 GPa	Wakelin *et al* [14]
Shear Modulus (film)	1.05 GPa -1.1 GPa	Leug *et al* [15]
Wave velocity (compression wave)*	$2345\,\mathrm{ms}^{-1}$	Habeger [9]
Wave velocity (compression wave)	$2620\,\mathrm{ms}^{-1}$	Mathieu and Schweitzer [16]
Density*	$1140\,\mathrm{kgm}^{-3}$	Rhodia Technical Fibers, Valence, France
Poisson's ratio* (bulk)	0.41	Goodfellow, Devon, USA
Loss tangent*	0.03	Leug *et al* [15]
Heat capacity	$1420\,\mathrm{Jkg^{\circ}K}$	Habeger [9]
Heat conductivity coefficient	$0.36\,\mathrm{Wm}^{-1}\mathrm{K}^{-1}$	Habeger [9]
Thermal expansivity	$6.0\text{e-}5\,\mathrm{K}^{-1}$	Habeger [9]

Table 3.3: Table of values for Nylon 66 and their source. The asterisk indicates values that have been used in the model.

7 Acknowlegments

I wish to thank to Swissflock for providing the fibres and Rhodia for the nylon fibre properties. My thanks go also to Jan Niemi and Jesper Martinsson for their support and their programming code.

References

[1] J. Levlin and L. Söderhjelm, *Pulp and Paper Testing*. Fapet Oy, 1999.

[2] D. Adams, *Ultrasonic transmission through paper fiber suspensions*. PhD thesis, University of London, 1975.

[3] P. Epstein and R. Carhart, "The absorption of sound in syspensions and emulsions. i. water fog in air," *The Journal of the Acoustical Society of America*, vol. 25, pp. 553–565, May 1953.

[4] J. Allegra and S. Hawley, "Attenation of sound in suspension and emulsions: Theory and experiments," *The Journal of the Acoustical Society of America*, vol. 51, pp. 1545–1564, 2 1972.

[5] A. Harker and J. Temple, "Velocity and attenuation of ultrsound in suspensions of particles in fluids," *Journal of Physics D: Applied Physics*, vol. 21, pp. 1576–1588, 1988.

[6] R. Challis, M. Povey, M. Mather, and A. Holmes, "Ultrasound techniques for characterizing colliodal dispersions," *Reports in Progress in Physics*, vol. 68, pp. 1541–1637, 2005.

[7] L. Flax and N. W., "Acoustic reflection from layered elastic absorptive cylinders," *Journal of the Acoustical Society of America*, vol. 61, pp. 307–312, Feb 1977.

[8] L. Flax, L. Dragonette, and H. Uberall, "Theory of elastic resonance excitation by sound scattering," *Journal of the Acoustical Society of America*, vol. 63, pp. 723–730, Mar 1978.

[9] C. Habeger, "The attenuation of ultrsound in dilute polymeric fiber suspensions," *Journal of Acoustical Society of America*, vol. 72, pp. 870–878, sep 1982.

[10] Y. Aitomäki and T. Löfqvist, "Measuring suspended fibre material properties by modelling ultrasound attenuation," in *Mathematical Modelling of Wave Phenomena*, 2005. To be published.

[11] J. Martinsson, *Statistical tools for ultrasonic analysis of dispersive fluids*. Licentiate thesis, Lulea University of Technology, 2005.

[12] A. Grennberg and M. Sandell, "Estimation of subsample time delay differences in narrowband ultrasonic echoes using the hilbert transform correlation," *IEEE Transactions on Ultrasonics, Ferroelectrics, and Frequency Control*, vol. 41, no. 5, pp. 588–595, 1994.

[13] L. Kinsler, A. Frey, A. Coppens, and J. Sanders, *Fundamentals of Acoustics*. John Wiley and Sons Inc., 4 ed. ed., 2000.

[14] J. Wakelin, E. Voong, D. Montgomery, and J. Dusenbury, "Vibroscope measurements of the elastic moduli of nylon 66 and dacron filaments of various draw ratios," *Journal of Applied Physics*, vol. 26, pp. 786–792, july 1955.

[15] L. W., K. Ho, and C. Choy, "Mechanical relaxations and moduli of oriented nylon 66 and nyon 6," *Journal of Polymer Science*, vol. 22, pp. 1173–1191, 1984.

[16] J. Mathieu and P. Schweitzer, "Measurement of liquid density by ultrasound backscattering analysis," *Meausurement Science and Technology*, vol. 15, pp. 869–876, 2004.

[17] C. Black and M. Dole, "Density of undrawn, drawn and annealed nylon filaments," *Journal of Polymer Science*, vol. 3, no. 3, pp. 353–364, 1948.

Paper D

Sounding Out Paper Pulp: Ultrasound Spectroscopy of Dilute Viscoelastic Fibre Suspensions

Authors:
Yvonne Aitomäki and Torbjörn Löfqvist

Reformatted version of paper originally published in:
Submitted to: Acoustics and ultrasonics in the processing of industrial soft solids

Sounding out Paper Pulp: Ultrasound Spectroscopy of Dilute Viscoelastic Fibre Suspensions

Yvonne Aitomäki and Torbjörn Löfqvist

Abstract

A model of attenuation of ultrasound in fibre suspensions is compared to a model of backscattering pressure from submersed cylinders subjected to a sound wave. This analysis is carried out in the region where the wavelength is of the same order as that of the diameter of the fibre. In addition we assume the cylinder scatterer to have no intrinsic attenuation and the longitudinal axis of the scatterer is assumed to be perpendicular to the direction of propagation of the incident wave. Peaks in the frequency response of both the backscattering pressure, expressed in the form of a form function, and the attenuation are shown to correspond. Similarities between the models are discussed. Since the peaks in the form function are due to resonance of the cylinder, we infer that the peaks in the attenuation are also due to resonance. The exact nature of the waves causing the resonance are still unclear however the first resonance peaks are related to the shear wave and hence the shear modulus of the material. The aim is to use the attenuation model for solving the inverse problem of calculating paper pulp material properties from attenuation measurements. The implications of these findings for paper pulp property estimation is that the supporting fluid could, if possible, be matched to density of that of pulp fibres and that the estimation of material properties should be improved by selecting a frequency range that in the region of the first resonance peaks.

1 Introduction

This study is part of a project aimed at the on-line characterisation of pulp fibres suspended in water, as used in the paper manufacturing industry. An analytical model was developed to relate ultrasound attenuation to the material properties of the fibre and the supporting fluid. This model was presented in [1]. This has then been used this to solve the inverse problem of estimating material properties from measurements of ultrasonic attenuation in dilute suspensions of viscoelastic fibres [2].

Experiments from these studies showed local peaks in the frequency response of the attenuation [1][2]. The focus of the study is on the cause of these peaks. A large body of work exists on attenuation due to suspended spherical particles, as reviewed in [3]. However, for cylindrical scatterers, much of the work has been based on backscattering and in the regime where the ratio of the wavelength to the diameter of the scatterer is small [4][5][6][7][8][9]. One of the theories arising from these works is the Resonance Scattering Theory (RST) [5]. This study compares the backscattering from theory developed for a

submersed cylinder [10] to a model of ultrasonic attenuation in a suspension of fibres in a fluid [1]. The theory developed by [10] is essentially the same as the nuclear scattering theory introduced in the derivation of the RST theory [5]. In this study we will use the rewritten version of [10] found in [11] since this matches the propagation direction of the wave used in the attenuation model.

Once a comparison of the resonance peaks is made, the explanation for the peaks in the backscattering is investigated to see if it is valid for the peaks found in the attenuation.

2 Theory

The attenuation is calculated from the simple cylinder scattering, (SCS), model [1]. The derivation of this model follows Habeger [12] cylindrical extension of the Epstein and Carhart [13]/Allegra Hawley [14] model. The resulting expression for the attenuation, α, of a suspension of fibres in a fluid of low viscosity, such as water is

$$\alpha = \frac{-2f_r}{\pi R^2 k} \Re \left(\int_0^{\frac{\pi}{2}} (\epsilon_n^2 B_n) \cos(\psi) d\psi \right), \tag{1}$$

where f_r is the volume fraction; R is the radius of the fibre; k is the wave number of the wave in water; ψ is the angle of the fibre to the direction of the oncoming plane ultrasound wave; $\epsilon_n = 1$, if $n = 0$, otherwise $\epsilon_n = 2$, and n is a positive integer. B_n are the n^{th} expansion coefficients of the wave potential of the reflected wave. The coefficients, B_n, are a function of the fluid properties: viscosity, density and speed of the compression wave and the fibre properties: shear modulus, density, loss tangent and speed of both the compression and the shear wave. The speed of the shear wave is a function of the shear modulus and the density and is related to the compression wave speed by Poisson's ratio.

For the purpose of the comparison between the attenuation and backscattering we assume that the axial plane of the fibres is perpendicular to the direction of propagation of the wave. Since we are focusing on the frequency at which the peaks occur we also assume that there is no intrinsic attenuation in the cylinder. This is done by setting the loss tangent to zero.

The expression for backscattering pressure from a cylinder at a large distance from the cylinder is

$$P_s \approx \sqrt{\frac{2a}{2r}} e^{ikr} f_\infty(\pi) \tag{2}$$

where P_s is the scattering pressure; a is the size of the scatterer and in this case equals R; r is the distance to the scatterer centre, k is the wave number of the wave in the fluid and $f_\infty(\pi)$ is the form function [10], [5].

The form function can be expressed using a phase shift expression, where the phase shift is that between the incident and reflected wave such that:

$$f_\infty(\pi) = \frac{2}{\sqrt{\pi k a}} \sum_{n=0}^{\infty} (-1)^n \epsilon_n \sin(\eta_n) e^{-i(\eta_n + \frac{3\pi}{4})} \tag{3}$$

where η_n is the phase shift [11] and is defined as,

$$\eta_n = \arctan\left[\tan\delta_n(ka)\frac{\tan\alpha_n(ka)+\tan\phi_n(k_La,k_Ta)}{\tan\beta_n(ka)+\tan\phi_n(k_La,k_Ta)}\right] \tag{4}$$

The following functions were used in the above equation:

$$\tan\alpha_n(x) = -x\frac{J_n'(x)}{J_n(x)}, \tag{5}$$

$$\tan\beta_n(x) = -x\frac{N_n'(x)}{N_n(x)}, \tag{6}$$

$$\tan\delta_n(x) = -x\frac{J_n(x)}{N_n(x)}, \tag{7}$$

$$\begin{aligned}\tan\phi_n(k_La,k_Ta) &= \frac{\rho_1(k_Ta)^2}{2\rho_2} \\ &\times \frac{\dfrac{\tan\alpha_n(k_La)}{\tan\alpha_n(k_La)+1} - \dfrac{n^2}{n^2-\dfrac{(k_Ta)^2}{2}+\tan\alpha_n(k_Ta)}}{\dfrac{n^2-\dfrac{(k_Ta)^2}{2}+\tan\alpha_n(k_La)}{\tan\alpha_n(k_La)+1} - \dfrac{n^2\cdot(\tan\alpha_n(k_Ta)+1)}{n^2-\dfrac{(k_Ta)^2}{2}+\tan\alpha_n(k_Ta)}}.\end{aligned} \tag{8}$$

Here, ρ_1 is the density of the water; ρ_2 is the density of the solid, k_T is the wave number of the shear wave in the solid; k_L is the wave number of the compression wave in the solid and n is a positive integer. J_n and N_n are Bessel function of the 1st kind and 2nd kind respectively, to the order n and J_n' and N_n' are the derivatives of the Bessel functions of the 1st kind and 2nd kind respectively, to the order n.

The frequency range is expressed in terms of normalised frequency $F_n = ka$, and we consider the range F_n from 0.2 to 5. The series expansion is truncated after eleven terms.

3 Results

The parameters in the models are set based on the material properties of Nylon 66 and water. However, as previously stated we are focusing on the frequency at which the peaks occur, so the loss tangent of the cylinder material is set to zero. To ease the comparison between the peaks in both backscattering and the attenuation, the amplitude of the attenuation is scaled and offset by 2 units. The results are presented in Figure 1.

Under these conditions there is a good match between the backscattering form function, $f_\infty(\pi)$ and the attenuation, α. The match between these two functions has two

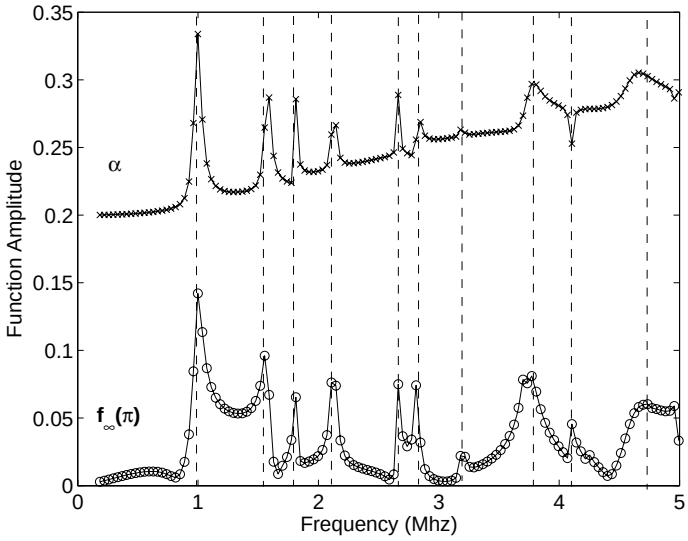

Figure 1: Plot of the acoustic attenuation, α, and the form function, $f_\infty(\pi)$, against normalised frequency for nylon fibres suspended in water. To ease the comparison between the peaks in both functions, the amplitude of the attenuation is scaled and offset by 2 units.

consequences. Firstly, the solution for the expansion coefficients used by Faran [10] can be used in the calculation of attenuation -equation (2) -instead of the solution for the expansion coefficient used in the attenuation. This results in a simpler solution as that used by Faran [10] uses slip boundary conditions. We can then compare the amplitudes of the attenuation calculated using the two different solutions for the expansion coefficients and hence the effects of the different boundary conditions. Work on this continues.

The second consequence of the match between the form function and the attenuation is that the resonance peaks in the form function have been well discussed, in both [10] and [6]. Faran [10] states that the normal modes of the cylinder are found when the normal component of the stress and the tangential component of the shear stress at the solid boundary are zero gives a condition which is identical to setting the denominator of Equation (8) to zero. Using this condition the normal modes can be calculated from Equation (8). Faran [10] also discusses that a shift in the resonance frequency of an immersed cylinder due to the reactive component of the acoustic impedance acting on the scatterer by the surrounding fluid. Although in his study this shift was small as the metal cylinders that were used had much greater densities than the surrounding fluid, in our case, where the density of nylon is close to that of water, the effect will be considerable. When calculating the normal mode for nylon, the first mode occurs at a normalised frequency of 1.4 (R = 44 μm, 7.8 MHz), however, the effect of the surrounding fluid moves this peak to a normalised frequency of 1.0 (R = 44 μm, 5.3 MHz). The

frequency can be found by setting the denominator in equation 4 to zero. Also discussed is the fact that the since the speed of the shear waves is much lower than the speed of the compression wave. The first modes to appear are from the shear wave. Since the $n = 0$ does not support shear waves, the frequency of this mode depends on the speed of the wave and hence occurs at a normalised frequency of 3.57 (R = 44 μm, 19.3 MHz). These calculations are for a cylinder with no loss.

Resonances in backscattering are explained as being caused by creeping waves in the fluid and in the solid [6]. However, the assumption used in these explanations is that the normalised frequency is much greater than 1, which is not the case here. Hence the actual wave propagation modes in this region of normalised frequency are still not clear.

4 Conclusion

From the results so far it appears that the coefficient derived by Faran [10] for backscattering can be used to derive attenuation. From this model, the resonance modes of a cylinder and a cylinder in water can be obtained. They confirm that the peaks in the attenuation curves are due to resonance. It appears as if the shear waves are causing first peaks in the ultrasound attenuation although the exact nature of these waves has not been established. These calculations have been done under the conditions of no loss.

The implication of these findings for the use of estimating material properties of paper pulp from ultrasound attenuation are that, if possible, the density of the surrounding fluid should be as close as possible to that of the suspended fibre. This increases the phase shift in the suspension and increases the dependency of the attenuation on the material properties of the fibre. The frequency range should also be set, if possible, so that resonance peaks exists within the range. Since the frequencies of the peaks depend on the material properties of the fibre, identifying these frequencies should aid in estimating material properties.

References

[1] Y. Aitomäki and T. Löfqvist, "Measuring suspended fibre material properties by modelling ultrasound attenuation," in *Mathematical Modelling of Wave Phenomena*, 2005. To be published.

[2] Y. Aitomäki, *Towards a measurement of paper pulp quality: ultrasonic spectroscopy of fibre suspensions*. Licentiate thesis, Luleå University of Technology, 2005.

[3] R. Challis, M. Povey, M. Mather, and A. Holmes, "Ultrasound techniques for characterizing colliodal dispersions," *Reports in Progress in Physics*, vol. 68, pp. 1541–1637, 2005.

[4] H. Uberall, G. Gaunaurd, and J. Diarmuid Murphy, "Acoustic surface wave pulses and the ringing of resonances," *Journal of the Acoustical Society of America*, vol. 72, pp. 1014–1017, Sept 1982.

[5] J. Diarmuid Murphy, J. George, A. Nagl, and H. Uberall, "Isolation of the resonant component in acoustic scattering from fluid-loaded elastic spherical shells," *Journal of the Acoustical Society of America*, vol. 65, pp. 368–373, Feb 1979.

[6] L. Flax, L. Dragonette, and H. Uberall, "Theory of elastic resonance excitation by sound scattering," *Journal of the Acoustical Society of America*, vol. 63, pp. 723–730, Mar 1978.

[7] H. Uberall, L. Dragonette, and L. Flax, "Relation between the creeping waves and the normal modes of vibration of a curved body," *Journal of the Acoustical Society of America*, vol. 61, pp. 711–715, Mar 1977.

[8] J. Dickey, G. Frisk, and H. Uberall, "Whispering gallery wave modes on elastic cylinders," *Journal of the Acoustical Society of America*, vol. 59, pp. 1339–1346, June 1976.

[9] G. Frisk, J. Dickey, and H. Uberall, "Surface wave modes on elastic cylinders," *Journal of the Acoustical Society of America*, vol. 58, pp. 996–1008, Nov 1975.

[10] J. Faran, "Sound scattering by solid cylinders and spheres," *Journal of the Acoustical Society of America*, vol. 23, pp. 405–418, July 1951.

[11] J. Mathieu and P. Schweitzer, "Measurement of liquid density by ultrasound backscattering analysis," *Meausurement Science and Technology*, vol. 15, pp. 869–876, 2004.

[12] C. Habeger, "The attenuation of ultrsound in dilute polymeric fiber suspensions," *Journal of Acoustical Society of America*, vol. 72, pp. 870–878, sep 1982.

[13] P. Epstein and R. Carhart, "The absorption of sound in syspensions and emulsions. i. water fog in air," *The Journal of the Acoustical Society of America*, vol. 25, pp. 553–565, May 1953.

[14] J. Allegra and S. Hawley, "Attenation of sound in suspension and emulsions: Theory and experiments," *The Journal of the Acoustical Society of America*, vol. 51, pp. 1545–1564, 2 1972.